UCONN LIBRARY

University of Connecticut
OpenCommons@UConn

Master's Theses | University of Connecticut Graduate School

9-12-2011

Understanding Formation and Transport of Amorphous Iron Oxyhydroxides in Porous Media using Microfluidic Flow Cells- a Novel Method to Study Freshwater Iron Cycling

Neha A. Ghaisas
neha.ghaisas@gmail.com

Recommended Citation
Ghaisas, Neha A., "Understanding Formation and Transport of Amorphous Iron Oxyhydroxides in Porous Media using Microfluidic Flow Cells- a Novel Method to Study Freshwater Iron Cycling" (2011). *Master's Theses*. 170.
https://opencommons.uconn.edu/gs_theses/170

This work is brought to you for free and open access by the University of Connecticut Graduate School at OpenCommons@UConn. It has been accepted for inclusion in Master's Theses by an authorized administrator of OpenCommons@UConn. For more information, please contact opencommons@uconn.edu.

Understanding Formation and Transport of Amorphous Iron Oxyhydroxides in Porous Media using Microfluidic Flow Cells- a Novel Method to Study Freshwater Iron Cycling

Neha Ajit Ghaisas

B.TECH; GGSIP University, New Delhi, 2006

A Thesis

Submitted in Partial Fulfillment of the

Requirements for the Degree of

Master of Science

At the

University of Connecticut

2011

APPROVAL PAGE

Master of Science Thesis

Understanding Formation and Transport of Amorphous Iron Oxyhydroxides in Porous Media using Microfluidic Flow Cells- a Novel Method to Study Freshwater Iron Cycling

Presented By

Neha Ajit Ghaisas, B.TECH.

Major Advisor_____

Dr. Allison A. MacKay

Associate Advisor _____

Dr. Leslie M. Shor

Associate Advisor _____

Dr. Joseph T. Bushey

University of Connecticut

2011

ACKNOWLEDGEMENTS

The continued enthusiasm and inspiration expressed by Prof. Allison MacKay throughout my association with her made this thesis possible. With her encouragement, sound advice and direction I was able to transform myself from an engineer to researcher.

I would like to express my gratitude towards Prof. Leslie Shor who introduced me to the world of microfluidics, Prof. Josheph Bushey for his support throughout my master research and Prof. McCutcheon for permission to access and utilize the SurPASS Electrokinetic Analyzer at the Fuel Cell Center, UCONN for significant experimental work. I would like to thank Liwei (PHD Student, Prof. McCutcheon) for providing the essential training for SurPASS Analyzer, Prof. Shor's group - Grant for fabrication of device masters, Andrea for AutoCAD, casting and Jessica for experimental setup.

I would also like to thank the Environmental Engineering program for their financial and academic support throughout my graduate work and the Center for Environmental Sciences and Engineering for their collaboration. Finally, I would like to recognize UCONN Research Fund and CESE Multidisciplinary Research Grant- Summer 2011 for the funding of this project.

I am indebted to my husband Saurabh, who encouraged me to pursue higher education and supported me throughout my years in graduate school. I am also thankful to my extended family that has been extremely supportive of my decision to study.

Lastly and most importantly, I wish to dedicate this thesis to my parents Shubhada Ghaisas and Ajit Ghaisas who cultivated the scientific temperament during my formative years that led to this thesis.

Table of Contents

List of Figures and Tables

(cont..)

Abstract

The ground water and surface water interface (GSI or Hyporheic zone) is a spatially- and temporally-fluctuating biogeochemical transition zone connecting these two distinct hydrological components. The mixing zone is characterized by a near neutral pH, ambient temperature and a sharp oxygen concentration which in turn has deep impact on the iron cycling and thus the fate of contaminants in the water column. We constructed an experimental micromodel that to observe key processes that affect biogeochemical iron cycling in the fresh water interface zones where the oxic surface water mixes with Fe (II) rich underlying ground water. The flow cell was constructed from Polydimethylsiloxane, (PDMS) a transparent, biologically inert silicone polymer which can be modified to represent the surface properties of natural porous media by oxygen plasma exposure. Our results demonstrated that with 25 seconds of high RF oxygen plasma exposure, the zeta potential of the PDMS surface is well within the reported range for other silicates and can be used as a surrogate for natural porous media. Using preformed iron oxide particles, a particle deposition rate of 415 min^{-1} and a single collector efficiency of 0.081 were obtained after PDMS "beads" had reached steady state coating. Iron oxide coating thicknesses on the PDMS beads were greatest at the inlet side of the flow cell and decreased in the flow direction toward the outlet. Reverse chemical gradients of dissolved Fe (II) and oxygen were created in a flow cell using a diffusive mixer to deliver source waters containing iron-only or oxygen-only solutions at circum-neutral pH. Subsequent monitoring of iron oxidation in the flow cell showed iron oxide particles to form and accumulate along the longitudinal center-line of the flow cell where the theoretical Fe (II) oxidation rate was calculated to be highest. Iron oxide particle accumulation in the flow cell was greatest around beads located at the inlet and decreased with distance along the flow path towards the outlet. These results indicate that PDMS micro-models may be used to simulate mixing zones in porous media, in particular the mixing of oxygen-rich water with anoxic iron- or metal-rich groundwater that represents an important aspect of biogeochemical iron cycling in the groundwater-surface water interface.

Introduction

Contaminant transport across the ground-surface water interface zone (GSI) has intrigued researchers for decades. The GSI also known as Hyporheic Zone, is a dynamic transition region between ground and surface water bodies where the concentrations of conservative solutes varies between 10 – 90% of their respective end zone concentrations [1]. European Geosciences Union (EGU) General Assembly adopted the following definition for the Hyporheic Zone: *"The saturated transition zone between surface water and groundwater bodies that derives its specific physical (e.g. water temperature) and biogeochemical (e.g. steep chemical gradients) characteristics from active mixing of surface and groundwater to provide a habitat and refugia for obligate and facultative species [2].* Advective exchange of nutrients and oxygen is governed by geomorphic features like surface roughness, permeability and soil composition which in turn drive the biochemical processes in the vertical profile of the interface [1]. Also, hydraulic conditions of the surface flow above the sediment govern the prevailing boundary conditions for the transport of reactive solutes and microbial activity [3]. The mixing zone is characterized by a near neutral pH, ambient temperature and availability of nutrients that allow the resident biota to utilize the metal transformation reactions for their energy requirements [4]. Modeling techniques have been employed in the past to characterize the physical parameters that drive water fluctuations and thermal disturbances in the GSI (or Hyporheic Zone). These models have been used to predict the ambient conditions that drive biogeochemical cycling of nutrients and contaminants [5, 6]. Large range of residence time of solutes in the interface zone arises from small scale heterogeneities in the sediment bed coupled with dynamic mixing of surface and ground water. A continuous time random walk model was used to simulate solute transport under varied residence times [7].

The fates of contaminants that are coupled to iron cycling are sensitive to gradients in the Hyporheic zone. Redox gradients in the GSI arise from the mixing of the two distinct water bodies. The Fe (II) /Fe (III) redox couple actively contributes towards the chemical speciation, bioavailability and mobility of contaminants occurring in the

environment. Groundwater often contains elevated concentrations of ferrous (Fe^{2+}) species [8].Mixing of such ground water with the oxygen-rich surface waters create a unique redox environment in the sediment-water interface where opposing concentration gradients of oxygen and the reduced species exist. The steep oxygen gradient existing in the vertical water column drives the important biochemical iron redox processes [9]. In the abundance of oxygen, dissolved Fe (II) species are abiotically oxidized to Fe (III). Although important, it can occur only in the shallow surficial sediments and the processes become biologically mediated moving a couple of centimeters below the surface water (Figure 1). Fe (II) oxidation under oxic conditions at circum-neutral pH either abiotic or biotic produces poorly soluble Fe (III) minerals that efficiently sequester metalloids such as Arsenic (As) and antimony (Sb). Fe (III) solids or HFO (hydrous ferrous oxides) s provide a large surface area for contaminant sequestration and can be employed as a potential remediation mechanism for removal of metalloids from the fresh water systems. Ability to utilize newly formed iron oxyhydroxides deposited by the IOB (iron oxidizing bacteria) as electron acceptors for IRB (iron reducing bacteria) opens the possibility to find coexisting colonies of IOB (iron oxidizing bacteria) and IRB (iron reducing bacteria) in environments that show a steep oxic to hypoxic to anoxic trend [10]. At near neutral pH, the half life of Fe (II) is between 2-10 minutes. Lithotrophic Fe(II) oxidizers compete with abiotic oxidation processes of Fe(II) for survival in the suboxic interface zone [11]. Microbial oxidation rates are directly related to the Fe (II) concentrations and are highest under low O_2. The abiotic: biotic Fe (II) oxidation ratio was observed to be highest in oxic environments. The IOB (iron oxidizing bacteria) community outcompete with chemo-oxidation of Fe(II) and hence are very difficult to characterize and isolate [12]. On the other hand, organisms using Fe(II) as electron donor under anoxic conditions have been well characterized [13]. The IRB (iron reducing bacteria) are abundant in anoxic regimes of sediment water interface and oxidize organic matter with Fe (III) as the terminal electron acceptor. These Fe(III) solids then precipitate in the oxygen deficient region of the GSI [14].

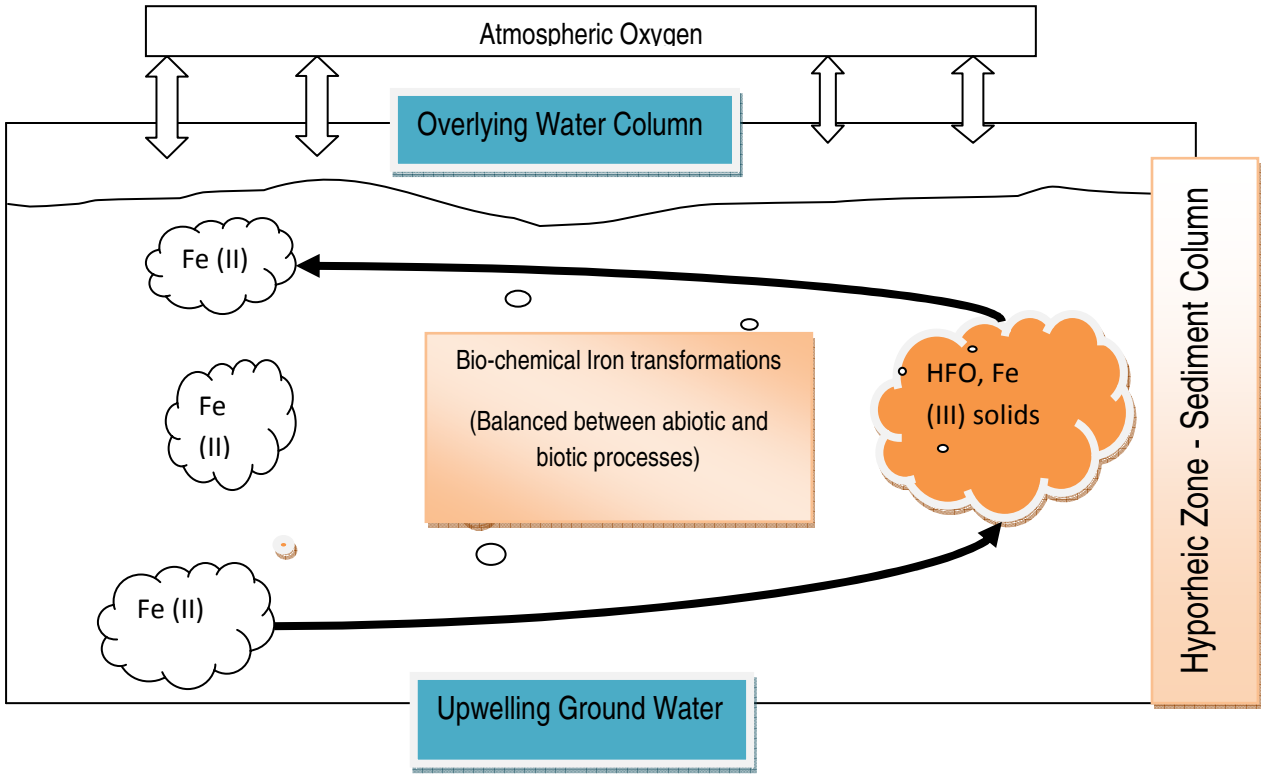

Figure 1: Conceptual representation of bio-chemical iron cycling in the Hyporheic Zone

The amorphous iron oxides produced as a result of abiotic (oxygen limited) or biotic (biologically mediated) processes have a large surface area which adsorbs and thereby transports arsenic. Dissolved arsenic concentrations in ground water were strongly related to the presence of iron solids which sorbed both As (III) and As (V). Simultaneous presence of dissolved As and Fe (II) concentrations in ground water demonstrated that microbial reduction of Fe(III) in the anoxic ground water repartitioned the sorbed As followed by transporting dissolved arsenic to distances away from source. Overall, the biogeochemical iron cycling plays a role in mobilization and fate of several contaminants [9].

Colloid-mediated contaminant transport has been the focus of research due to an observed translocation of and appearance of contaminants at a much larger distance from their known sources.

Previously, contaminant transport was based on a two phase ground water system consisting of an immobile solid phase and a mobile aqueous phase wherein, the mobility of contaminants in the subsurface aqueous region was

dependent entirely on the partitioning of the contaminant between the two phases. According to this theory, a greater extent of partitioning into the immobile phase would indicate slower average transport velocity and vice versa. Unexpected appearance of contaminants at some distance away from the known source gave rise to the three phase ground water distribution system which took into account enhancement in contaminant transport mediated by colloids present in the natural porous media. Three phases, the mobile fluid phase, immobile solid phase and a mobile colloid phase were found to exist in the subsurface aqueous environments. The mobile colloid phase was found to consist of sub micron-size clay particles, iron oxyhydroxides, silica, natural organic matter, viruses and bacteria [15]. Identified sources of mobile colloids include in situ mobilization of naturally occurring particles, precipitation from super-saturated solutions, and introduction from landfill seepage, septic tanks or ground water recharge.

Laboratory studies have been done in the past to demonstrate colloid- mediated transport in the subsurface aqueous zone. These studies were able to demonstrate the active role of clay minerals, silica and hematite in transporting heavy and trace metals through porous media. The typical representation of porous media here was done using quartz sand, glass beads, sand/soil column or Ottawa sand. Field studies of colloid-mediated contaminant transport across natural porous media have successfully demonstrated the role of silicates, iron oxyhydroxides in transporting trace and heavy metals [16].

Present day freeze core sampling techniques obtain snap shots of biogeochemical interactions that take place at the GSI. The conventional methods are able to obtain in situ spatial and temporal distribution of the prevailing nutrients and contaminants inside the media impacted GSI. Gan et al demonstrated the sequestration of ground water arsenic into nearby sediments by sorption onto amorphous oxides which were formed during the iron redox transformations occurring in a landfill leachate impacted GSI [17]. The combined use of freeze core and bead column sampling method succeeded in providing centimeter- scale resolution of sediment phase Arsenic and iron oxide concentration as governed by the prevailing biogeochemical processes occurring at the test site.

Freeze core sampling methods were employed to quantify arsenic and solid phase iron concentration from the test site along with characterization of the predominant microbial community profiles. IOB and IRB densities were calculated for the different depths of the site and the results confirmed the role of iron oxidizing and reducing bacteria in the iron transformation. Bead column sampling method (wherein glass beads were inserted into the water column for a period of minimum 29 days) was used to calculate the mass deposition rates of iron oxide and of arsenic sorption on a well characterized substrate media. The retrieved bead columns exhibited rust-colored staining on the glass beads indicating the role of iron oxide- silica interactions that provided a background for understanding the transport of the arsenic containing Fe (III) solids through the GSI [17].

Limitations of conventional sampling methods included -determination of only the average concentration for the sections, steep concentration gradients within unobserved regions and mixing within the extracted samples leading to disturbances in concentration profiles. The surface characteristics of the glass beads likely differ from the sediment media in the GSI zone. Also, the short deployment times (average 29 days) of the bead columns might limit the extent to which biological processes affect contaminant distributions on the bead surfaces. Conventional ground water sampling techniques used to study colloid transport have been used in the past. The major concern here is the effect of perturbations on the colloids due to pumping of ground water. Submicron-size colloids can be mobilized by the hydrodynamic shear introduced while sampling [18]. The question then arises whether such techniques can truly represent the mixing induced interactions leading to colloid transport.

Micromodel flow and transport systems are excellent platforms for elucidating coupled processes involving advection, diffusion, and biogeochemical reactions at the pore-scale, and for providing insights to continuum-scale processes. The velocity profiles found in the field can be easily measured and by scaling down these values to fit into a millimeter resolution micromodel, field processes can be viewed under the microscope.

A transparent arrangement of pores and constrictions that simulate some of the complexities of natural porous media which can be utilized to observe microscale flow and transport processes by identifying and describing mechanisms at pore level. Chatenever and Calhoun (1952) were the first research group to utilize a visual

approach for investigating processes in the porous media. Recent micro models utilize the microfluidic systems that are fabricated in glass or silica (Si/SiO2). Using the micromachining and photolithography techniques, the microscopic channels can be defined on the substrates. Past research provided evidence for usability of these materials as surrogates for natural porous media. Glass bead micromodel has been utilized in the past to study solute transport in the porous media (Corapcioglu et al 1997). Microfluidic pore structure etched on a silicon wafer was used for analyzing transverse mixing induced calcium carbonate precipitation under super-saturated conditions [19]. There is large body of data available to justify the success of glass and silica based micro models [19-22].

The major limitations here include cost and rapid development and testing of silicon/glass based microfluidic devices. The fabrication techniques are very similar to the semi conductor industry. The use of these materials for environmental applications is limited and not cost efficient as they are fragile and expensive to dispose off after single experiments (an approach common to most experimental studies). Silicon being optically opaque cannot be used for observing pore-scale processes under the microscope. Semiconducting properties of silicon reduce its usability for microfluidic applications where particle interactions are predominated by electromagnetic fields. Overall, although silicon has proved very useful in the microelectronic applications, there are several properties that require costly modification techniques before it can be used a substrate for microfluidic applications [23].

Polymers, specifically silicone elastomer (Polydimethylsiloxane) offer a low cost, mechanically robust alternative to glass and silicon, as a substrate for microfluidic devices. With rapid and inexpensive fabrication techniques, these polymers can be used to construct multiple microfluidic devices in less time. The 3-D micro channels, pores and constrictions can be designed using AutoCAD or any other open source design software. The design can be printed onto a master printed using soft photolithography. Multiple devices can be cast from a single silicon master. These devices can be plasma bonded to glass slides to seal the channels. Plasma bonding also renders the surface hydrophilic, a property useful for numerous environmental applications.

Limitations of using PDMS for microfluidic applications arise due to the loss of hydrophilic properties when exposed to dry air which require the micro channels to be filled with water in order to preserve the hydrophilic property. Once plasma bonded to glass, the PDMS cannot be peeled off from the glass slide. Clearly, the ease of design and the rapid, low cost fabrication of these PDMS based microfluidic devices outweigh the limitations arising from irreversible plasma bonding.

Objectives

The dynamic nature of the ground-surface water interface (GSI) gives rise to a variety of biogeochemical processes that affect transport of conservative solutes. Insufficient modeling and experimental techniques are available to measure flow and residence time distribution of water. While conventional sampling techniques are employed to observe macro scale changes arising from these processes, a better approach to observe microscopic pore-scale processes at real time is needed. The interactions between the products of biochemical processes with the solid phase porous media have challenged many researchers to develop efficient contaminant remediation strategies. Packed glass beads have been utilized in the past as a surrogate for natural porous media. Micromodels developed so far (Silicon wafer) are able to simulate the conditions as they would exist at microscopic scales but require expensive construction techniques. In this research, we propose to use Polydimethylsiloxane as a cost efficient substitute material for Silicon wafer or glass beads.

The purpose of this project is to provide answers to the following questions:

1. Can PDMS replicate surface properties of natural porous media particles?
2. Can we simulate the iron adsorption kinetics within the porous media as seen in previous research[17]?
3. Can we demonstrate the mixing observed in the Hyporheic zone at a transverse scale with known gradients?
4. Can we observe real time iron cycling as observed in the field?

Organization of Thesis

The four questions identified in the project objective have been answered in separate sections. The first section provides a comprehensive analytical and experimental justification for using PDMS as a surrogate material for natural porous media due to its similar chemical composition and surface properties. We have attempted to demonstrate that plasma oxidation, a method integral to microfluidic device fabrication is an effective technique to match the surface zeta potential of PDMS with reported results for different forms of silica that have been used for colloidal contaminant transport studies. This method served as background support for our iron transport experiments. The second section discusses the particle interactions between the silica surface and iron oxyhydroxides. Using the classical clean bed filtration theory, we were able to successfully observe sub micron scale particle interactions between the surface of PDMS and iron oxides. The design of engineered porous media-Ecochip consisted of microstructures similar to those found in the natural porous media. Adsorption experiments simulated the process by which iron oxides are transported through porous media due to surface interactions. The third section provides an experimental Flow Cell design based on diffusive mixing. This microfluidic device consisted of a scaled version of the Ecochip connected to a two input –diffusive mixing channel. We were able to successfully set up a chemical gradient inside the porous media induced by diffusive mixing of the two inlet solutions. The purpose of using food dyes was to quantify the mixing pattern visually and anticipate expected concentrations along the width of the porous media. Finally, the fourth section provides a comprehensive view of iron oxidation kinetics inside the porous media under a diffusive mixing regime. With this section we were able to collectively demonstrate processes that govern iron oxidation and transport of amorphous iron oxides across an engineered porous media as a simulation of field observations.

Surface Characterization of Polydimethylsiloxane (PDMS)

Brief overview

The primary objective of the surface characterization of PDMS was to evaluate whether the surface chemistry of PDMS was similar to that of natural porous media. The zeta potential is a measure of the surface potential of the solid surfaces and can be used to characterize the surface of PDMS and compare it to different forms of silica. Most of the suspended particles typically found in natural aquifers are negatively charged in neutral pH range. The presence of ionizable functional groups (-OH) give rise to chemical reactions between the solid phase and dissolved electrolytes in the aquifers. For silica particles, neutral Si-OH groups on the surface can undergo the following proton exchange reactions:

$\equiv Si\text{-}OH_2^+ = \equiv SiOH + H^+ (aq)$ Ka1 (1)

$\equiv SiOH = \equiv SiO^- + H^+ (aq)$ Ka2 (2)

Where ≡ denotes surface bound species , Ka1 and Ka2 are equilibrium constants.

The magnitude of net positive or negative charge on the silica surface is mediated by the pH of the surrounding solution phase due to the extent of prevailing proton transfer mechanism (discussed later). The total net particle charge on a suspended solid is denoted by σ_p (unit –surface charge density: Coulomb m^{-2}). This charge is the sum total of charges arising from permanent structural charge, net proton charge (dependent on the pH of solution) and inner and outer complex charges (arising from hydrogen bonding or London-van der Waals surface interactions) [24].

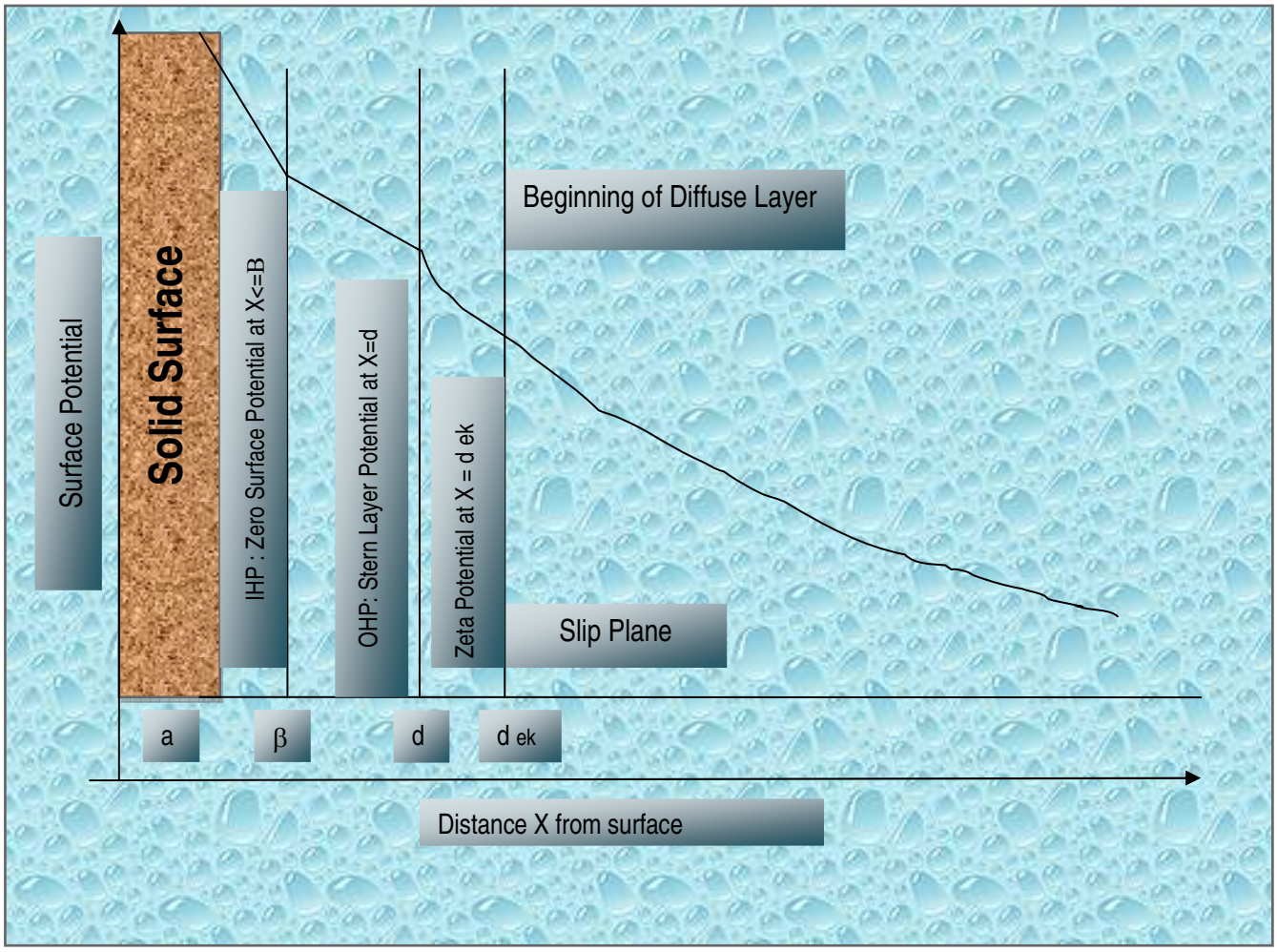

Figure 2a: Conceptual distribution of surface potential along distance X from the solid surface

For a given surface (of initial width 'a' units) in contact with an electrolyte, there is spatial distribution of the total surface charge density which gives rise to the electrical double layer around the solid surface. The double layer (EDL) consists of two components – fixed (Stern) layer attached to the surface and diffuse layer to maintain electrostatic equilibrium (Figure 2a).The fixed layer (Stern Layer) can be further subdivided into an inner Helmholtz layer (IHL), bounded by the surface and the inner Helmholtz plane (IHP) ($0<X<\beta$) and an outer Helmholtz layer (OHL), located between the IHP and the outer Helmholtz plane (OHP) ($\beta<X<d_{ek}$) [25].

The Gouy-Chapman theory defines the relationship between surface charge density (σ_p) and surface potential (ψ) (volts) in water (dielectric constant $\varepsilon = 78.5$) at 25°C as

$$\sigma_p = 0.1174 * (c)^{1/2} \sinh (Z \psi * 19.46) \qquad (3)$$

Where c is the molar electrolyte concentration and Z is the charge of the ion.

The thickness (κ) of the EDL is a parameter to understand the drop in surface potential (ψ) at a distance from the surface. At ($\psi < 25$mV), the drop in potential is given by the following relationship:

$$\psi = \psi_0 \exp (-\kappa d) \qquad (4)$$

The surface potential cannot be experimentally determined since it is impossible to connect an isolated solid particle to any electrical measurement circuit. Applying external electrical or mechanical force can cause tangential flow of liquid along the charged solid surface. Under this flow motion, a very thin layer of fluid adheres to the surface. The thickness of this layer extends to d_{ek} (Figure 2a). This hydrodynamic system assumes a pseudo-particle system such that the new solid surface has a width of ($a + d_{ek}$) (if the initial solid surface width was a). The sharp boundary between the above hydrodynamic pseudo-particle and mobile fluid phase is called the Shear Plane. With known applied force, the surface potential, now known as Electro kinetic Potential or ζ- potential can be measured at this shear plane.

Origin of Surface Charge on PDMS

PDMS is a polymer with the chemical formula **CH_3---[$(CH_3)_2$---Si---O)]$_n$----$(CH_3)_3$.**The presence of Si—O_2 groups on the surface of PDMS makes it similar to natural sediments which are largely constituted of Si—O_2. The active sites on these silica irrespective of its type or origin (natural sediments, glass, PDMS) are Si—OH groups. When the PDMS solid surface is in contact with an aqueous KCl solution, at a given pH, the positive ions (H^+, K^+) preferentially concentrate around the negatively charged solid surface. This charge separation leads to the

formation of an Electrical Double Layer. A conceptual figure below is shown to indicate the charge organization and resulting surface potential distribution that occurs when a solid PDMS surface is in contact with an aqueous electrolyte. As the distance from the surface increases, the surface potential (ψ) drops exponentially. The ζ is measured along the shear plane by measuring the electrophoretic mobility of the moving charged particles.

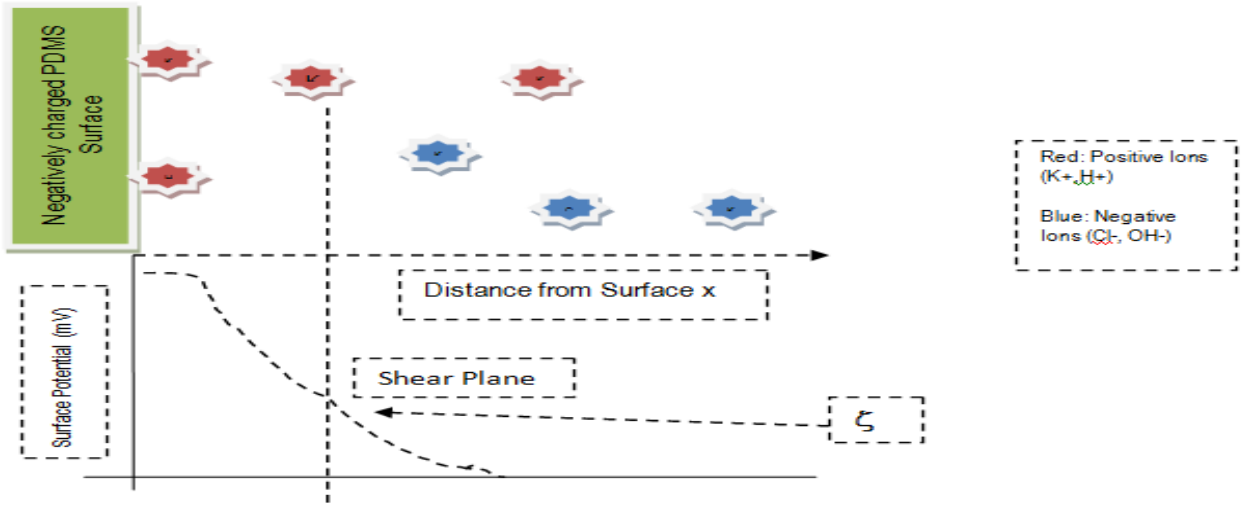

Figure 2b: Conceptual Figure –Charge Distribution and Shear Plane. (Not to Scale)

Zeta Potential Measurement Principle

Application of either an external electric field (electro-osmosis, electrophoresis) or applied mechanical force (streaming potential/current), can cause the fluids to flow tangentially over the solid surface as discussed. The Smoluchowski's theory can be applied for all non conducting solids independent of their shape and size provided the particle size (a) (Figure 2a) >>> Debye Length (κ^{-1}) such that $\kappa a >>> 1$. Under this assumption, the tangential liquid flow arises purely from the tangential component of the applied force and is independent of the EDL. The EDL is assumed to be negligible compared to the size of the solid surface. Streaming current / potential are phenomena that occur inside capillaries and plugs causing charge displacement in the EDL as a result of an applied pressure. This induces the liquid phase to move tangentially to the solid.

Significance of pH in Zeta potential Measurements

A solid surface in contact with a mobile liquid phase develops the EDL (Figure 2a). The mobile liquid phase is characterized by a pH that represents the distribution of H^+ and OH^- ions in the solution. The ionic strength and pH of the solution in contact with the silica surface together regulate the magnitude of positive or negative charge. At equilibrium, the number of positive or negative charge sites per unit surface area is equal. The pH of the solution phase which sets the system to equilibrium is called the point of zero charge or $p_{zc.}$ The zeta potential at this pH value is 0. The iso-electric point is the pH value characteristic of the mineral surface where no adsorption takes place and the only potential determining ions are H^+ and OH^- .For naturally occurring silica minerals, the reactions at the surface of silica (1 and 2) have equilibrium constants K_{a1} and K_{a2}. The point of zero charge can be calculated as $(pK_{a1} + pK_{a2})/2$. Titration methods have been used for decades, along with electrophoretic mobility, to gain surface charge (or potential) data that have been tremendously useful in understanding surface properties of the mineral surface. The value of iso electric point for silicates occurring in natural sediments has been reported to range from 2 – 4 due to variation in chemical compositions of the different minerals [26-28]. On increasing the pH above the iso electric point, the excess hydroxyl ions around the solid surface contribute to a net negative charge which leads to an increase in the zeta potential value. In order to incorporate all natural aquifer pH range, surface characterization experiments for our study was limited to a pH titration over a range 5-8.

Effect of Plasma Oxidation on PDMS

The presence of Si-OH groups on the surface of PDMS in contact with an aqueous medium gives rise to a charge distribution thus resulting in a surface potential. When this surface is exposed to high power RF oxygen plasma, the reaction between the excited oxygen molecules and the PDMS surface leads to the formation of a thin SiOx layer on the exposed surface. The surface of PDMS consists of a long chain polymer consisting of repeating

CH_3--- $[(CH_3)_2$---Si---O)$]_n$---- $(CH_3)_3$. When this surface is exposed to excited oxygen molecules (O=O-O^-), the Si-CH3 bonds are broken and replaced with Si-OH bonds which render the surface electronegative. At high RF intensity, increasing the exposure time of the surface actually increased the concentration of oxygen plasma in contact with the surface thereby increasing the thickness of this SiOx layer. The consecutive increase in the SiOx layer thereby increases the associated active Si-OH sites leading to an increase in the zeta potential value of the surface. The formation of the oxide layer is directly proportional to the exposure time associated with the surface [29]. The thickness of this oxide layer, although related to plasma exposure time, has a stress limit beyond which the surface becomes brittle and oozing of polymer from subsurface layers leads to surface hydrophobicity. Neutron reflectometry and XPS studies done on spin coated PDMS exposed to Oxygen Plasma, MW radiations indicate the formation of 130-160nm thick smooth oxidized SiOx layer over the exposed surface. The SiO2 content was reported to increase with increased exposure times thereby increasing the active sites on the surfaces [30]. Overexposure to oxygen plasma causes progressive oxidation of the surface and renders the top silica layer brittle [31].Reported results indicate that around 100 seconds of exposure time, microscopic cracking of the surfaces would be observed. Parameters of plasma oxidation system like RF power, amount of exposed oxygen plasma and time of exposure together define the surface stability of PDMS due to differences in the surface reaction rates.

Methods

Analytical

The streaming current can be detected directly by measuring upstream and downstream electric current using an electrometer, non polarizable electrodes and low resistance setup. SurPASS Analyzer is an instrument that works on the streaming potential l/current measurement method. For a known pressure drop, Δp and the measured streaming current I_{str}, *Helmholtz-Smoluchowski Equation is given by,*

$$\zeta = \frac{Istr}{\Delta p} * \frac{\eta}{\epsilon * \epsilon_0} * \frac{L}{A * R} \qquad (5.1)$$

Where

ζ–Zeta Potential

$\eta 0$–.Electrolyte Viscosity

$\varepsilon 0$-Vacuum Permittivity

ε-Dielectric Constant of Electrolyte

L-Length of Streaming Channel

A-Cross Section Area of streaming channel

R-Ohm Resistance inside the measuring cell

The SurPASS Electrokinetic Analyzer (Anton-Paar, Electrokinetic Analyzer for Solid Surface Analysis: SurPASS) uses this approach for calculation of zeta potential of planar PDMS sheets, glass slides that are mounted on the Clamping Cell Arrangement. (Appendix 3) *(An extension of Helmholtz-Smoluchowski Equation is Fairbrother Mastin Method, f*or particles of irregular geometry and small size where the zeta potential can be calculated from the streaming potential and specific electrical conductivity of the electrolyte solution.

$$\frac{L}{A} = k * R \qquad (5.2)$$

Where

κ-.Specific electrical conductivity of the solution inside the capillary system

$$\zeta = \frac{Istr}{\Delta p} * \frac{n}{\epsilon * \epsilon_0} * \kappa \qquad (5.3)$$

The Fairbrother Mastin method is used for samples of irregular geometry and small size (> 25 microns) which can be packed into the Cylindrical cell Arrangement. (Appendix 3)

Materials

Background Electrolyte (0.001M Potassium Chloride solution) used for all Electro kinetic Measurements was prepared from Potassium Chloride Crystalline (Mol. Wt 74.55 g/mol) dissolved in DI water . All pH titrations were performed with 0.1M NaOH and 0.1M HCl solutions.

Sample Preparation

PDMS and Curing agent from Sylgard (R) 184 Silicone Elastomeric Kit (which includes Base and Curing Agent) from Dow Corning Corporation, Midland, MI were prepared mixing in a 10:1 base to curing agent ratio for preparing the PDMS samples for different studies. (Appendix 2)

Effect of oxygen plasma exposure on zeta potential

PDMS prepared according to the above mentioned procedure was poured into separate sterile petridishes and was cured in the oven at 60^{o}C for at least 2 hours. Four different samples were cut to the SurPASS Analyzer specified dimensions (**55mm X 25mm X 2mm**) to be measured with the clamping cell. Sample 1 was not plasma activated, Sample 2 was plasma activated inside the Plasma Cleaner (Harrick Plasma Cleaner, Model #: PDC-32G) for **25 seconds** by mounting on the glass slides**,** Sample 3 for **30 seconds** and Sample 4 for **60 seconds** respectively. The RF valve of the plasma cleaner was carefully turned to its full capacity for every sample in order to maintain uniformity of oxygen plasma exposure. Following plasma activation, all samples were stored in DI water continuously to retain the hydrophilic properties. Extreme care was taken to ensure minimum exposure to dry conditions prior to the experiments.

Effect of sample geometry on zeta potential

PDMS prepared similar to the previous experimental setup was poured into 2 separate sterile petridishes and allowed to cure in the oven at 60^{o}C for at least 2 hours. Sample 1 was cut to the SurPASS Analyzer specified dimensions **(55mm X 25mm X 2mm)** to be measured with the clamping cell. Sample 2 was cut into approximate 2mm cubes that would be measured with the cylindrical cell. Both the samples were plasma activated inside the Harrick Plasma Cleaner for **25 seconds** each by mounting on glass slides. They were immediately submerged in DI water till the experiments were performed. Sample 1 being a planar sample was mounted on the Clamping Cell setup of the analyzer. Sample 2 were packed into the Cylindrical Cell setup of the analyzer as these were individual 2mm cubes.

Compare Different Forms of Silica with 25 Sec Plasma Cleaned PDMS

The final set of samples consisted of different forms of silica that have been used for representing natural porous media. Ottawa Sand (baked at 400^{O}C), Sterile Glass Beads (2mm diameter) and an untreated Concrete Sand sample from Desiato's Sand and Gravel, Storrs CT were used in order to cross compare with the plasma activated PDMS planar samples. There was no special treatment procedure performed for the samples used in this experiment set. Each sample was packed into the Cylindrical Cell due to their size and run on the analyzer.

Obtain zeta potentials as a function of pH with a continuous titrimetric method

The pH titrimetric method was used to observe the trend of zeta potential values over the defined pH range 5-8 for each sample that was tested. Initial pH of the background electrolyte was adjusted to 4.0 and SurPASS Analyzer was allowed to run manually which allowed to instrument to add fixed volumes of 0.1M NaOH solution in order to increase the pH by 0.5 units before each measurement was taken.

Results and Discussion

Effect of Plasma Exposure Time

Plasma oxidation times of 0, 25, 30 and 60 seconds were examined with fresh PDMS samples. ζ decreases for all the samples when titrated over increasing pH (Figure 3). This trend is consistent with increasing –O-H groups on the solid surface. ζ were increasingly more negative with increasing length of time for plasma activation. For surfaces not exposed to plasma, the values ranged between -8.5 to -13.8 mV and for surfaces exposed to 25-30 seconds of plasma, the observed values were between -19.5 to -32.6 mV approximately. On exposing the surface to more than 60 seconds, there was an observed increase in the negative charge on the surfaces which ranged between -28.5 to -50 mV.

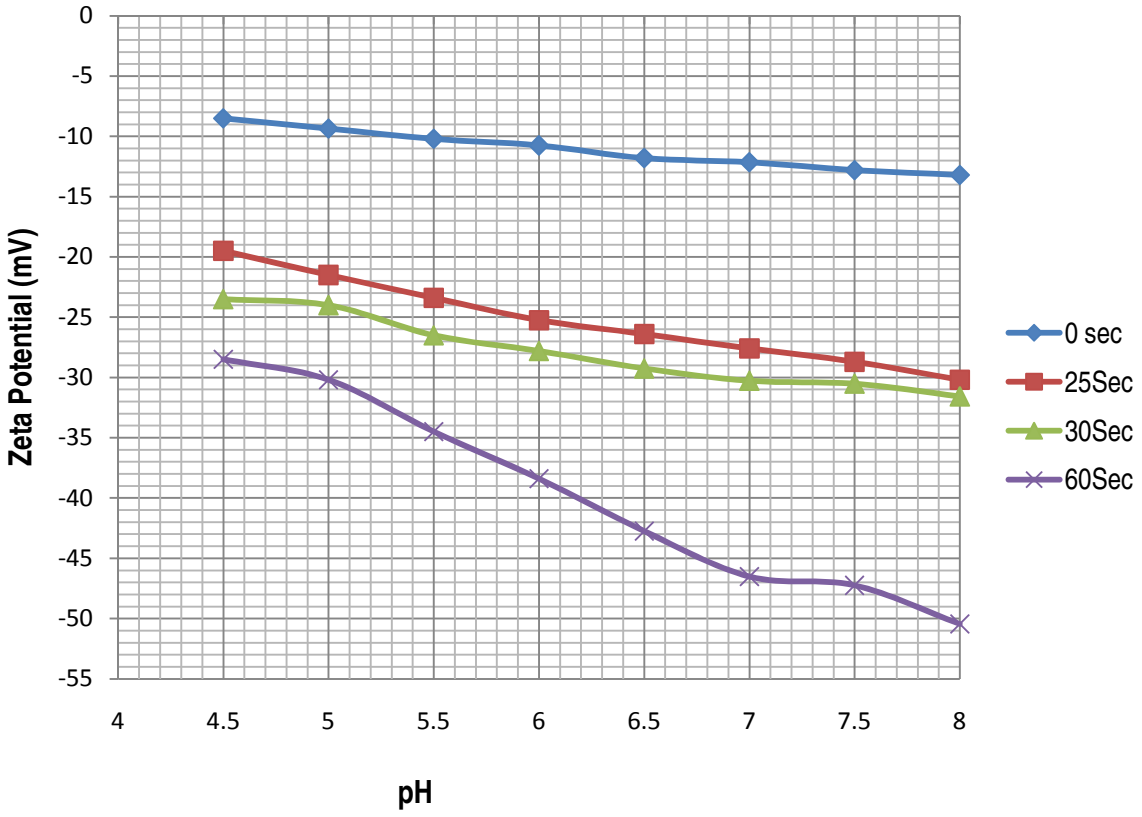

Figure 3: Observed effect of increasing plasma treatment time on zeta potential. Each sample was cut to dimension of -55mmX 25mmX 2mm and exposed to oxygen plasma for varying durations.

Effect of Sample Geometry on Zeta Potential

Natural porous media is granular rather than a single planar structure hence a better correlation of properties of natural sediment particles with PDMS required a comparative analysis of zeta potential for the same material cut to different shapes. Our study indicates that for the same amount (25 Sec) of plasma exposure time, the ζ potential of the planar sample ranged between -19.5 to -30.2 mV whereas ζ potential of the 2mm cubes of PDMS ranged between -23.5 to -31.57 mV (Figure 4). For the same exposure time, the cubes demonstrate a very small decrease in ζ potential values of the cubes compared to the planar sample. The relative increase in the values could have been due to a larger surface exposed to oxygen plasma in case of cubes. This test allowed us to confirm the usability of PDMS material as a representation of natural porous media.

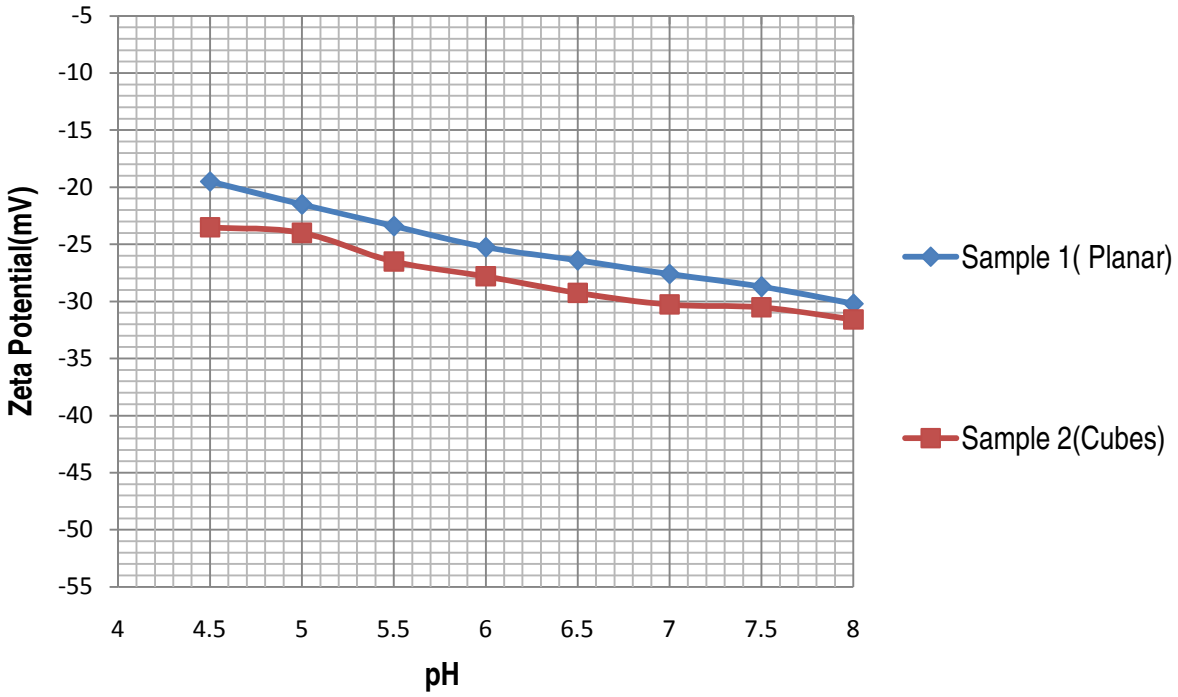

Figure 4: Observed effect of geometry of PDMS surfaces (treated with Oxygen Plasma for 25 sec each) on the zeta potential. Sample 1 was a planar sample (55mm X 25 mm X 2mm) mounted on Clamping Cell setup and Sample 2 consisted of 2mm cubes packed into the Cylindrical Cell setup.

Comparison between Different Forms of Silica and 25 Sec Plasma Cleaned PDMS

The final set of experiments was preformed to validate the reliability of using PDMS as a surrogate for natural porous media. The ζ potential value of an untreated Concrete Sand from Desiato's Sand and Gravel, Storrs CT ranged between -11.5 to -24.3 mV. Ottawa Sand (baked at 400°C) ranged between -14.8 to -26.63 mV, sterile Glass beads ranged between -20.5 to -28.3mV. Comparison of these values with Planar Plasma Cleaned sample for 25seconds (-21.5 to -30.2 mV) indicate that an exposure time of 25 seconds matched the ζ potential of the PDMS to a value that approximately matched the different forms of silica.

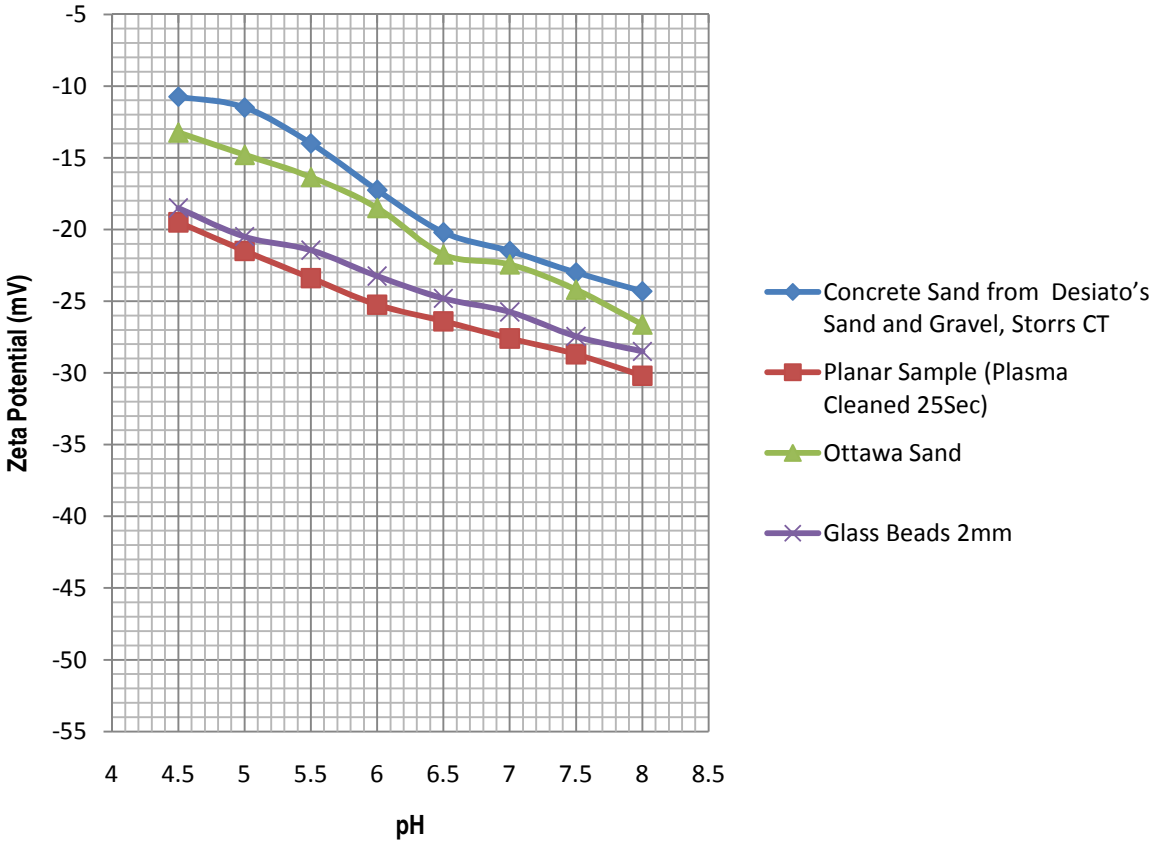

Figure 5: Comparison of 25 second plasma charged PDMS sample with different forms of silica

In a comprehensive review, consolidated ζ vs. pH relationship for different forms of silica based on data collected by different research groups , reported a range (-21 to -45mV) similar to our results [32]. It is to be noted that these results are a compilation of different studies and have been normalized for varied background electrolyte concentrations. Also, the values reported above are for different forms of silica and not PDMS exactly. Another study reported a similar ζ potential range between -20mV to -40mV approximately for natural (uncharacterized) porous media [33]. The ζ potential values reported for glass microscopic slides range between -45 to -75mV approximately which are observed to be different than other reported values for borosilicate glass (~-100mV approx.) [34]. Our data indicates that 25 seconds of plasma treatment of PDMS surfaces lies within the range of zeta potential values reported for different forms of silica that are also being used to fabricate microfluidic devices. Plasma treatment of PDMS is an important step required for bonding the microfluidic device to the glass slide prior to setting up any experiment. The surface characterization experiments allowed us to utilize plasma bonding as an important step required not only to build the device but to simulate surface properties that would allow the following adsorption reactions to proceed as they would in packed natural media. Although the conditions cannot be exactly replicated in the device as they would have in the field, PDMS would relate closely to natural porous media and allow us to observe processes that have been only coarsely represented through glass beads micromodel experiments in the past.

Transport of iron oxyhydroxides inside engineered porous media

Brief overview

Transport of the poorly soluble amorphous iron oxyhydroxides in granular porous media is of fundamental importance for contaminant removal from natural aquifers. The mobility of these colloids is controlled by the physic-chemical interactions between the particles and the media; which in turn are strongly dependent on the surface charge and solution chemistry[35]. Mobile colloids found in the subsurface aqueous environments consist of sub micron-size clay particles, iron oxyhydroxides, silica, natural organic matter, viruses and bacteria[15]. Identified sources of mobile colloids include in situ mobilization of naturally occurring particles, precipitation from super-saturated solutions, and introduction from landfill seepage, septic tanks or ground water recharge. An understanding of adsorption kinetics in the artificial porous media and compare with reported results for natural porous media is needed in order to develop robust contaminant removal techniques. In the previous segment, we were able to identify zeta potential as a deterministic property to relate surface characteristics of plasma cleaned PDMS with results reported for natural porous media. In this section, we will use Ecochip- an artificial porous media designed in AutoCAD and fabricated with soft lithography as a representation of natural porous media. Apart from the surface similarities, construction of the physical microstructure inside this microfluidic device demonstrates a porosity that is within the range of natural porous media which in turn would represent the physical structure characteristics of the porous media.

The deposition of suspended iron oxyhydroxides inside natural porous media can be described by accounting for particle advection, hydrodynamic dispersion, and deposition (filtration). In case of zero interactions between the particles, the physical mechanisms governing transport are filtration (entrapment), sedimentation (gravity) and settling. The two basic steps involved can be characterized as transport of particles from the suspension into the solid-liquid interface and attachment of the particles to the porous media entities (soil grain). Particles less that 1 micron in average diameter, demonstrate Brownian motion owing to thermal energies

generated during collisions. Particles larger than 1 micron in diameter on the other hand are mobilized by the fluid shear forces. Attachment of particles to the media is dependent on the particle-particle interactions that may be either of physical or electrostatic origin. [36]

In natural porous media, colloid deposition follows first order kinetics and can be explained with the classical filtration theory[37]. Electrophoresis mobility studies on iron oxide coated surfaces indicate that these oxides carry a net positive charge which leads the attractive interactions between the positively charged iron oxides and negatively charged silica surfaces. With no pre formed iron oxides already deposited on the porous media, all interactions are attractive (α=1) thus allowing the porous media to act as a clean bed filter. For relatively low particle concentration and moderate ionic strength, blocking and ripening effects are not significant and particle release is typically negligible. Mathematically, the concentrations of fluid-phase particles, C(x, t), and retained particles, S(x, t), at column depth x and time t can be described by a one-dimensional advection-dispersion equation with a first-order kinetic deposition term [22, 37, 38].

$$\frac{dC}{dt}\left(1+\frac{\rho_b}{f}\right)=\frac{Dd^2C}{dx^2}-\frac{vdC}{dx} \qquad (6.1)$$

$$\frac{\frac{\rho_b}{f}dS}{dt}=kC \qquad (6.2)$$

Where v is the particle velocity; D is the hydrodynamic dispersion coefficient, f is the bed porosity,

ρ is the porous medium bulk density and k is the particle deposition rate coefficient[39].

Assuming steady state system with negligible dispersion, at constant particle deposition rate (min^{-1}), the single-collector removal efficiency, η is obtained using the relation:

$$k=\frac{3(1-f)\eta}{2d} \qquad (6.3)$$

Methods

Ecochip Construction

Multiple Ecochip were constructed according to the standard procedure (Appendix 1) which contained the pores and constrictions to simulate the porous media.

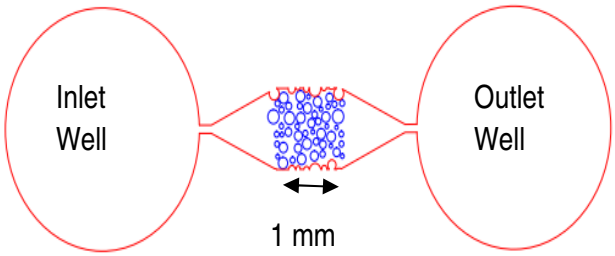

Figure 6: AutoCAD drawing for Ecochip Device showing the porous media in the center and the inlet and outlet wells

Materials

Amorphous Iron Oxyhydroxides were prepared by dissolving iron (III) nitrate nanohydrate (Acros Organics CAS# 7782-61-8; LOT# A0279517) in DI water according to the standard method [40]. Potassium hydroxide (Fisher Scientific CAS# 1310-58-3; LOT# 106388) was dissolved in DI water to obtain a 1M solution which was then added drop wise to the iron (III) solution until the final pH of the solution reached 7.27. The resultant solution was centrifuged 5 times to concentrate the iron solids. A suspension of iron (III) solid was prepared by stirring in 6.386 g of the refrigerated iron solids into 1L DI water. The resultant pale yellow suspension was then filtered through coarse P8 grade qualitative filter paper (Particle Retention: 20-25microns). The final concentration of this stock was found to be 21 mg / L of total iron measured by acid digestion and UV spectrophotometric detection [41].

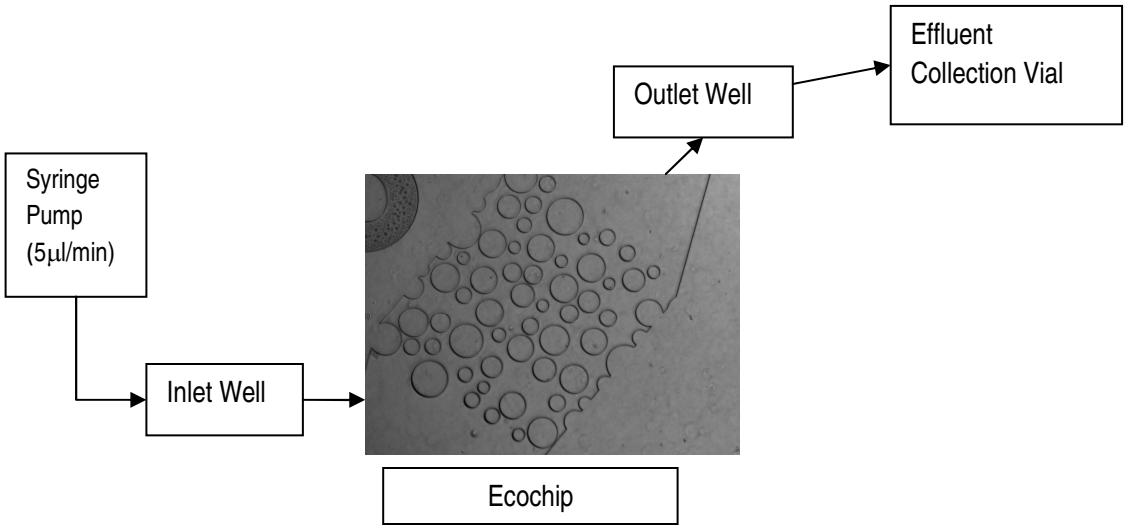

Figure 7: Experimental set up for iron colloid transport experiments indicating relative influent and effluent flow with an influent flow rate (5 μl/min)

Syringe pump (KD Scientific) was set up to flow at a fixed rate of 5μl/min. Tube fittings(Warner Instruments Cat # 64-1568 and 64-1576) were used to connect the 3ml BDL disposable syringes to the HPLC tube (1/8th inch ID) and in turn fitted into the inlet of the Ecochip. Similar tubing arrangement was set up to collect the effluent iron solution in a sterile Nalgene 1.5ml vials (Figure 7) Sterile 3 ml syringe was filled up with the Iron (III) stock while ensuring that no air bubbles entered the flow path. The experiment was allowed to run for a total of 180 minutes in order to obtain sufficient effluent for quantification of total iron. Mass balance of the influent and effluent were performed using the ferrozine method to quantify the amount of iron collected inside the Ecochip.

UV Spectrophotometric Analysis of Iron Concentrations

The Fe (III) was reduced to Fe (II) by acid digestion followed by adding excess 2.8M hydroxylamine solution. Ferrozine Standard solution was prepared by dissolving 0.257 g of Ferrozine and 5 g of $NH_2OH.HCl$ in 50 ml DI water. Acetate Buffer (pH=5.5) was prepared by dissolving 20 g (CH_3COONH_4) and 17.5 g (NH_4OH) in 50 ml DI water. The samples were prepared by mixing the iron containing sample, ferrozine reagent and acetate buffer in

the 50:1:1 ratio. The concentrations were measured by recording the Abs value at 562 nm (Peak Wavelength for Fe(II) detection) using the UV visible spectrophotometer[41].

Analytical

Adobe Photoshop CS5.1 (trial version) was used to obtain iron deposition trends inside the Ecochip from microscope camera images. The image captured prior to the start of the experiment was used as the background or baseline image for all calculations (Figure 9 (0 min)) The total count of "beads" was obtained using the 'Count Tool' in order to obtain the number of particles inside the Ecochip (Appendix 2) . Images captured at times 0, 30, 60, 90, 120, 180 minutes of the experiment were processed using this tool to identify number of beads coated with iron solids out of the total number of beads. Each image was zoomed to a resolution that allowed easy distinction between the sharp black perimeter of the bead and glass like iron particles around it (Figure 8). Using Count Tool, the beads demonstrating greater that 50% iron deposition around their surface were marked. A total count of marked beads was then obtained for each image. Dividing by the total number of beads inside the eco chip (obtained from background image), relative percentage growth was obtained. The particle deposition equilibrium curve for our experiment was obtained by this method.

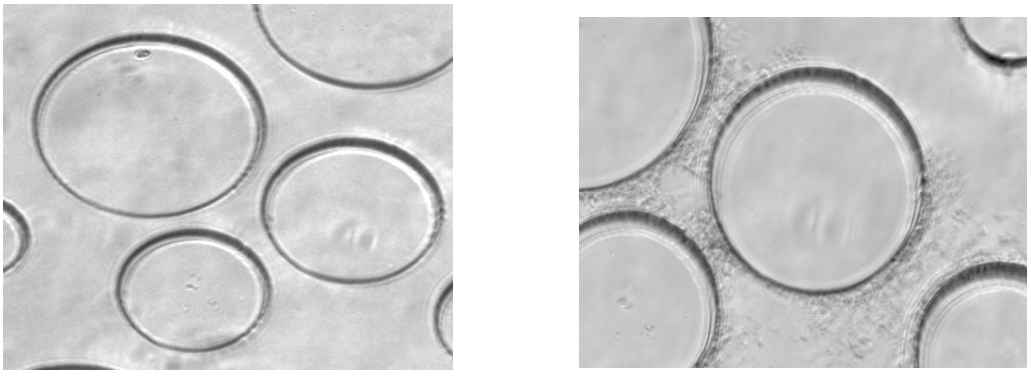

Figure 8: Magnified Images to demonstrate difference between uncoated and coated bead

Another set of data obtained from the final image (Figure 9, time 180 min) was the spatial iron deposition inside the Ecochip at the end of the experiment. The Ecochip length was divided into 5 segments of 0.2 mm thickness extending through the entire width of the Ecochip. Inside each segment, the net increase in bead diameter following the adsorption experiment was obtained using the 'Measurement' feature of Adobe Photoshop. An average of increase in radii in each segment was obtained in order to study the iron oxide spatial adsorption trend.

Results and Discussion

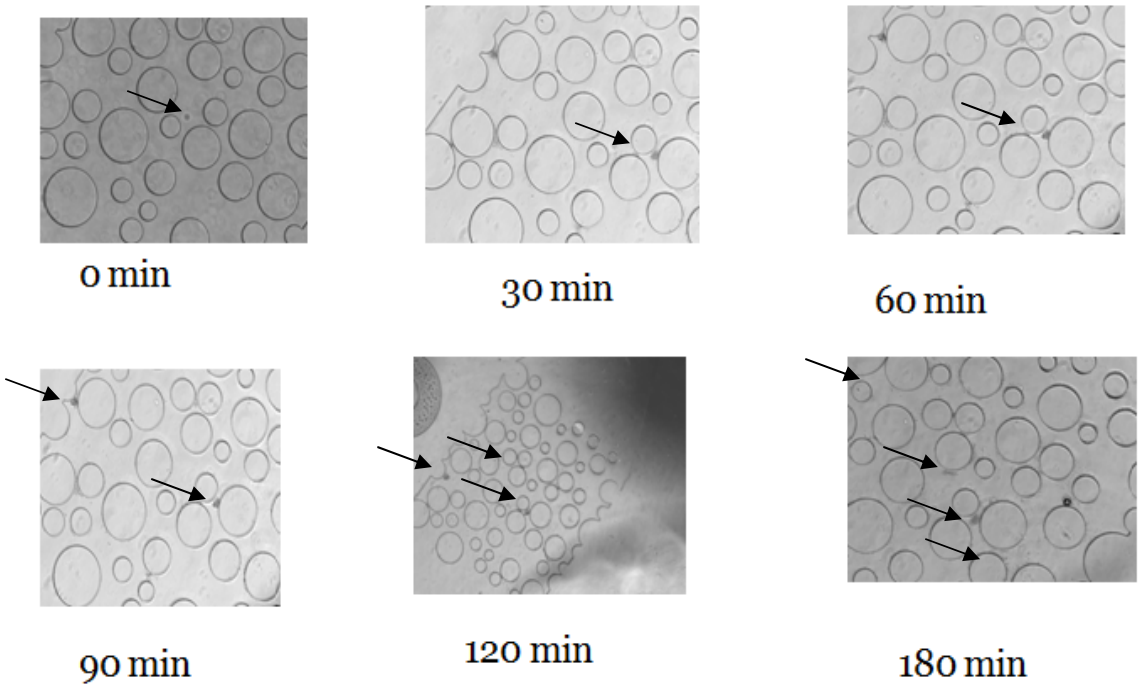

Figure 9: Iron Deposition images captured at different experiment run times (Pre formed iron oxides at pH 7.27 flowing across the porous media) Arrows point to observed iron deposition; Low resolution and amorphous nature of iron solids resulted in low contrast of images but were detected as orange staining when viewed under eyepiece of the microscope

The increase in iron oxide deposition around the “beads” over the duration of the experiment was observed over the entire duration of the experiment (Figure 9). It is important to note that due to the amorphous nature of iron oxides, the images captured by the monochrome camera of the microscope did not have a sharp contrast to detect iron oxide coating over the “beads” in comparison to the sharp edges of the bead itself. Although, when viewed under the eye pieces, the locations depicted with arrows contained glass like orange staining around the beads.

At t=0 min, the syringe pump started dispensing filtered iron stock into the inlet well. The solids had not reached the porous media and image shown above indicates a clean porous media. At t=30 min, there was particle deposition observed around the beads near the inlet. The flow of the influent iron oxyhydroxides particle (identified under the eye piece view as iron particles due to the orange color) was observed under the microscope. Particles were seen to collide and stick to the “bead” walls. Some particles started forming aggregates around the beads. At t=60 min, there was an observed increase in the number of “beads” coated with iron oxyhydroxides in comparison to the images collected at earlier experiment times. After t=90 min, the number of beads coated with iron were increasing. Aggregation of iron solids led to saturation of some pore throats. At t=120 minutes, all the beads inside the porous media were coated with iron oxyhydroxides. This was confirmed by viewing the Ecochip under the eye piece to compare with the monochrome images. The experiment was stopped at 180 minutes in order to analyze the effluent.

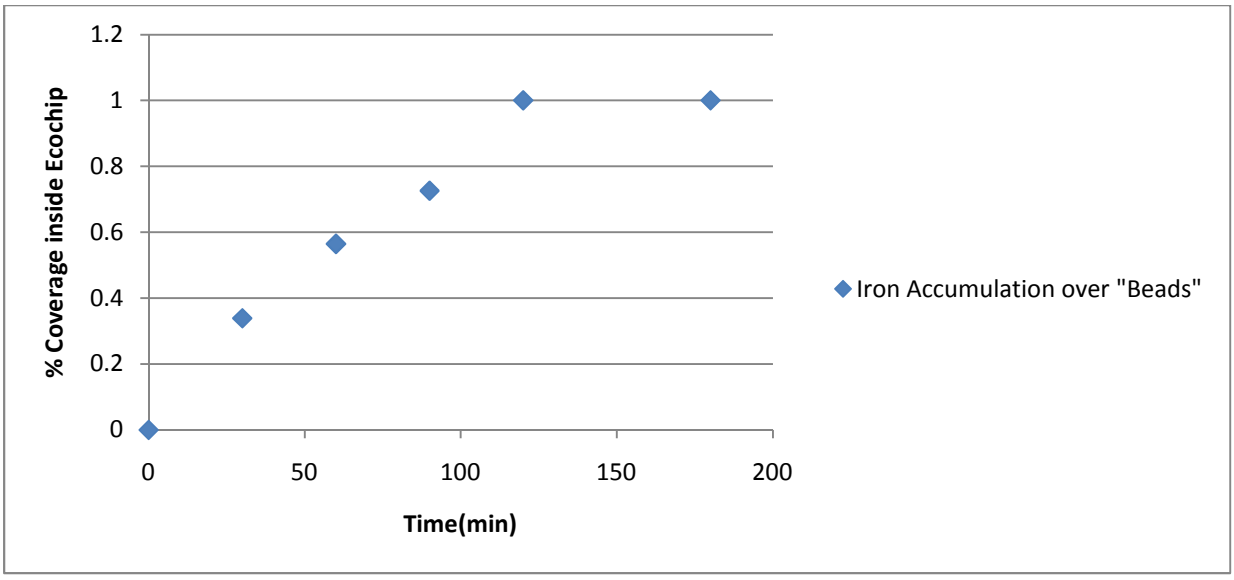

Figure 10: Observed trend for iron deposition around "Beads" over experimental run time (Image analysis to calculate % increase in coated /uncoated bead ratio; total number of "beads" 62). The equilibrium criterion for the experiment was the time taken for all beads to be coated with iron solids.

The particle deposition curve was obtained from the ratio of iron coated beads to total number of beads by analyzing the images (Methods) taken at different time intervals over the entire experiment duration. Our observation indicates that with a flow rate of 5μl/min, we were able to observe an equilibrium condition indicated by complete coverage of all beads inside the Ecochip device with visible and iron deposits after 180 minutes of experiment run time. This allowed us to perform spectrophotometric detection of the effluent to calculate the total iron concentration retained in solution at the end of the experiment.

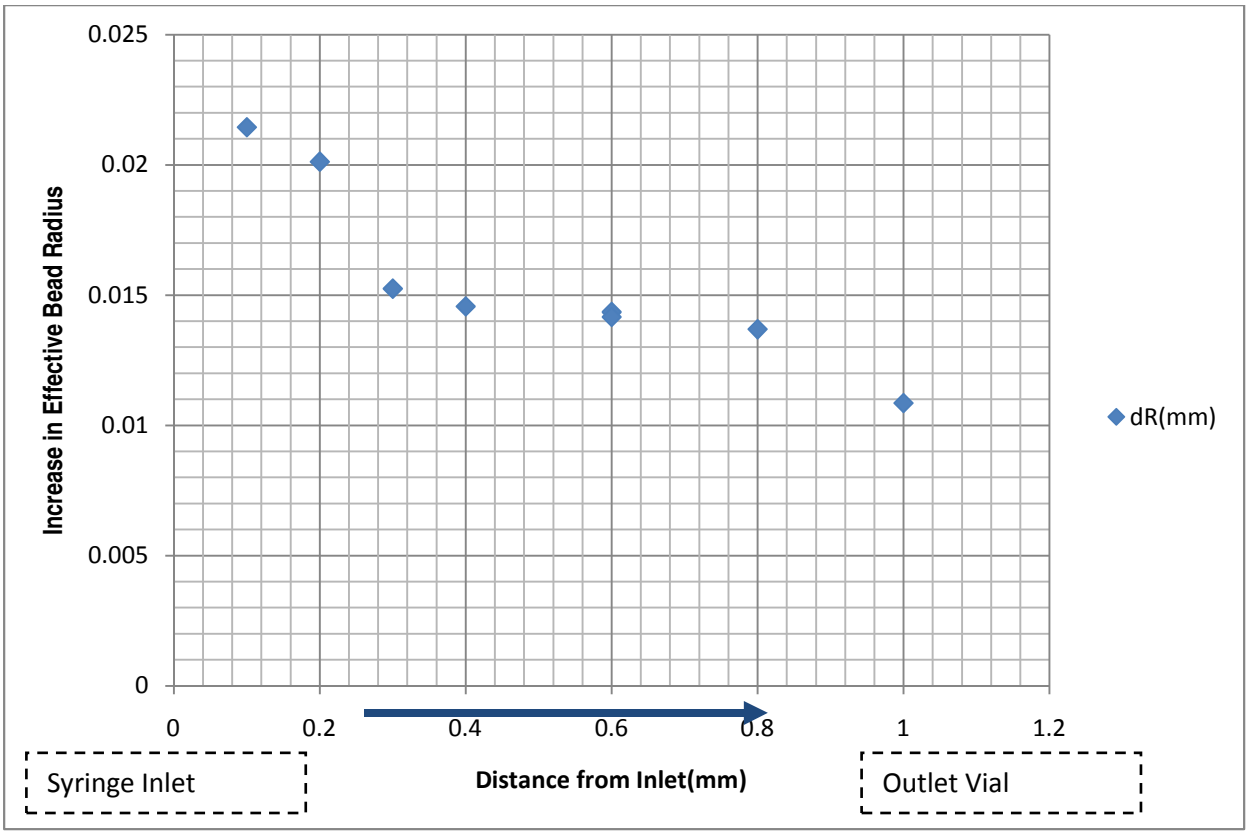

Figure 11: Spatial distribution of relative iron coating inside the Ecochip at the end of adsorption experiments. The Ecochip was divided into 0.2mm wide segments and average change in bead radius was measured using Adobe Photoshop for all beads inside each segment.

The bead diameter increased due to iron oxide coating formed around during adsorption (Figure 10). It was observed that the particles close to the source had larger accumulation around their surface compared to the particles located near the outlet. With the knowledge of surface chemistry of PDMS, it could be rationalized that the particles close to the source were observed to have larger coating of iron oxide due to the iron-PDMS surface interactions that attracted the positively charged iron species towards the negatively charged PDMS surface. It is likely that the pore throats near the inlet were saturated with iron oxyhydroxides due to interception of the new iron solids flowing inside. Predominance of attractive forces over advective transport near the source could explain the occurrence of more iron coating near the source as compared to the outlet.

Electrostatic interactions between the colloid particles and collector grains lead to dual deposition rates demonstrated particles wherein some particles preferentially attach faster to the collector while some particles show slow attachments[38]. The iron deposition around PDMS beads leveled off after 120 minutes and the experiments were stopped at 180 minutes of total run time. According to our results, this time was short in order to observe the change in interactive forces between the iron solids and 'beads". We believe that by running the experiment beyond the leveling off time, the presence of positively charged iron oxide coating over the beads would alter the net attractive forces inside the Ecochip.

The image analysis technique was to understand temporal variation in iron transport inside the artificial porous media which needed to be verified with a mass balance of the iron oxides in the influent and effluent samples. An observed increase in iron coating with respect to time only confirmed the usability of PDMS material as a surrogate for artificial media. The design of Ecochip was a simulation of particle spacing as observed in coarse sediments (Porosity ~ 49%). The flow rate used for our experiments was 5 μl/min resulted in an effective Velocity of Approach 337 mm/min. (Appendix 2). The interception area of the Ecochip was calculated as a product of length and width of the Ecochip. The Absorbance values obtained from UV spectrophotometry of influent (C_{in}) and effluent (C_{out}) samples were **0.1085** and **0.0582** respectively. These values were average of 3 runs of experiments performed on fresh Ecochips. The decrease in the concentration was consistent with the increase in iron deposition inside the Ecochip. Known flow rates and experiment run times allowed us to estimate the amount of iron adsorbed inside the Ecochip based on the first order adsorption kinetics.

The **(C_{out}/C_{in})** obtained from the above experiment was used to calculate the colloid deposition rate and single collector removal efficiency for the iron oxide-PDMS system [38] [39]. The experiment was performed with a clean Ecochip thereby allowing us to assume α =1. From the classical filtration theory discussed previously, the spherical packed bed collector efficiency was calculated using the relation below:

$$\eta = \ln (Cout/Cin)*d / ((3/2)*(1-f)*L) \quad (6.5)$$

$$k = \frac{3*\boldsymbol{\eta}*v}{2d} \quad (6.3)$$

Calculation parameters

C_{out}/C_{in}	0.5364055
$Ln(C_{out}/Cin)$	-0.6228648
α	1
d(diameter of grain)	0.099 mm
L(length)	1 mm
f(bed porosity)	0.4943
v(approach velocity)	337 mm/min

Our results indicate that the particle deposition rate coefficient (k) was 415 (min^{-1}) and single collector removal efficiency (η) was 0.0813 for the experiment. It is to be noted that the adsorption behavior observed inside the Ecochip would differ from what is observed in the field since the surface chemistry of PDMS is not identical to the natural porous media. Also, even though the flow rates and iron stock concentration were calculated to be within the natural aquifer limits, were adjusted according to the relatively small geometry of the Ecochip. We have not accounted for effect of turbulence in our iron transport experiments.

Diffusive mixing to create a chemical gradient in the cell

Brief overview

With a comprehensive understanding of surface chemistry of PDMS and the resulting interactions between the surfaces of PDMS and amorphous iron oxyhydroxides from previous experiments, particle interactions inside porous media were captured in the Ecochip. However, in order to truly represent the dynamic nature of the natural aquifers, there is a need to demonstrate the above surface interactions by incorporating the biogeochemical iron cycling processes. We have selected the Hyporheic zone as the natural aquifer regime to study mixing induced chemical reactions that lead to fresh water iron cycling. A detailed overview of the dynamic nature of this zone has already been discussed. Typical flow rate for ground water movement is 1ft /day and the hydraulic gradient is 0.005 to 0.01. With these values, the flow ground water velocity can be calculated using the Darcy's Law (Velocity $_{GW}$ = (hydraulic conductivity * hydraulic gradient)/ porosity) as 0.5 to 50 feet /day. The low velocities coupled with from small scale heterogeneities in the sediment bed coupled at the interface of surface and ground waters; provide a large range of residence time for diffusive mixing induced nutrient cycling.

Microfluidic devices are extensively used to manipulate distribution of chemical species under the two basic assumptions. Firstly, the concentration gradient set up inside is low enough for assuming uniform density/viscosity inside the device. Secondly, migration of charged chemical species under the effect of external electric fields is assumed to be negligible relative to the bulk motion of the fluid. The micro fabrication techniques employed for construction allow the transport mechanism inside the device to reside in the Low Reynolds –High Peclet Number regime.

The Peclet Number for a dilute species *x* of diffusivities *Dx*, diffusing over a characteristic length *l* with a transverse velocity *U*, is given by the relation

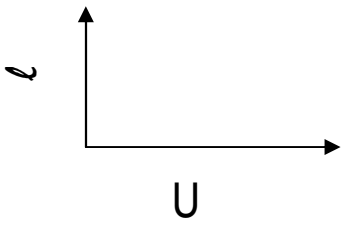

$$Pe = U*l / Dx \qquad (6.6)$$

Typically, particle diffusivities at 298K, for particles of radius, a, and fluid viscosity, η, can be obtained from Stokes-Einstein relation ($D = k_BT/6\pi\eta a$) where k_B is the Boltzmann constant. The values range between 10^{-9} - 10^{-17} which results in very high Peclet numbers for the flows of biochemical analyte particles. For effective diffusion of these species, the flow direction should be transverse to the diffusive length which occurs for Low Reynolds Number given by

$$Re = \rho * U * l / \eta \qquad (6.7)$$

The Reynolds Number for microfluidic applications is low, indicating laminar flow inside these devices[32]. Under these conditions, flow patterning can be used to predict the relative concentration of the analyte species along the characteristic diffusive length l, inside the microfluidic devices, the 1D diffusion of species with concentration C over length l and diffusivity D,can be described by the following equation

$$dC/dt = D * \frac{d2C}{dx2} \qquad 0<x<l \qquad (6.8)$$

The solution of this equation is given by

$$c = \frac{c\infty}{2} * erfc(\frac{x}{2*sqrt(D*t)}) \qquad (6.9)$$

Thus, for $x = l_{diff} \rightarrow$ sqrt (D*t), the concentration has reached halfway through equilibrium and is thus referred to as the characteristic diffusive length. For diffusive mixing to occur, the solution needs to flow over the length $l = l_{diff}$ for time t which is given by $(l_{diff})^{2}/D$. For microfluidic applications, this time would exceed the feasible experimental conditions. In order to achieve maximum mixing within feasible time range, the characteristic diffusion length scales. This is achieved by incorporating tortuous channels throughout the flow path with the use of Baker's transformations[32] (http://www.kirbyresearch.com/textbook).

The preliminary study after the design of the flow was complete was to see observe the concentration gradient inside the porous media using food dyes as tracers. This purpose of these experiments was to identify the different mixing ratios across the width of the porous media as this would enable us to predict the concentrations of reactants in the diffusion controlled reaction kinetics experiments performed inside these flow cells.

Methods

Flow Cell Construction

The Flow Cell was constructed with a diffusive mixing channel containing the tortuous paths to maximize the mixing of 2 inlet solutions. Also, with the large mixing channels, the porous media had to be enlarged in design to proportionally fit with the mixing scheme. The porous media was enlarged and scaled from the Ecochip design having the similar porosity and distribution of pores and constriction but the overall size of the cell was not increased to 10mm * 10mm* 0.017mm. Consequently the average diameter of the "beads" also was doubled in order to maintain the porosity. The fabrication steps were similar to Ecochip casting. (Appendix 1)

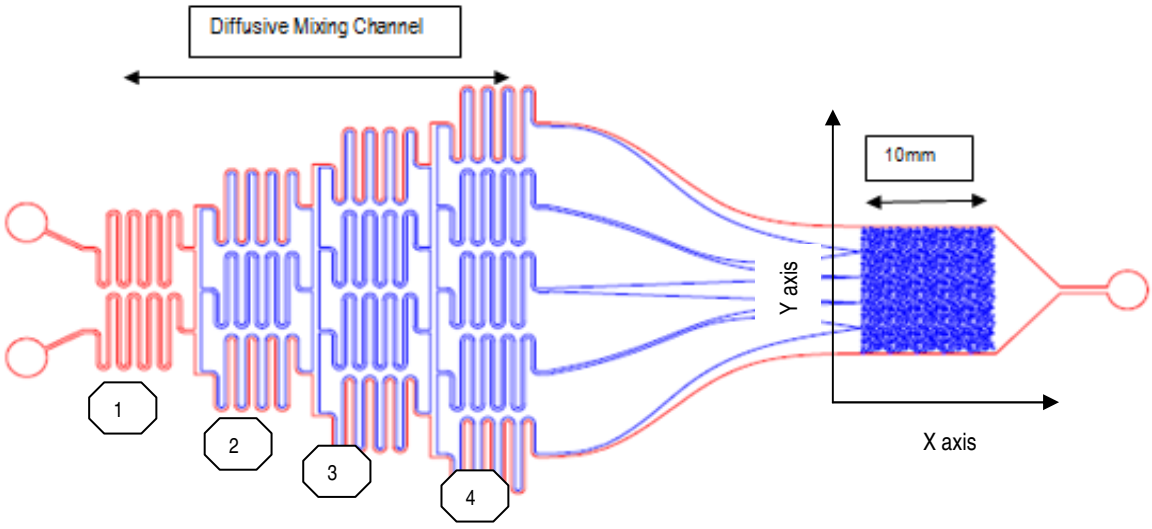

Figure 12: AutoCAD drawing of Flow Cell – for diffusive mixing chemical gradient showing segments of mixing channel (indicative markers placed on each segment; Y axis- characteristic diffusive length; X axis- Direction of flow)

The diffusive mixing channel was designed according to the previously discussed Baker's transformations. The reason for anticipated progressive increase in mixing as the flow moved from inlet toward the porous media along segments 1,2,3,4 was due to the lateral flow patterning between outlets of one segment and inlet of the subsequent along with sharp bends within a segment.

Experimental Setup:

The blank flow cell was first flushed with blank background (5mM) NaCl solution for 60 min to remove the air bubbles out of the device. Two new syringes were filled with concentrated Red and Yellow food color to perform the mixing tracer test. Each syringe was connected to a 1/8th inch ID HPLC tube as inlet into the diffusive mixer. The entire set up was carefully connected such that there were no air bubbles in the entire flow regime including

the porous media. The syringe pump was set up flow at a rate of 5μl/min and both the syringes were set up to dispense at the same time. (Figure 12)

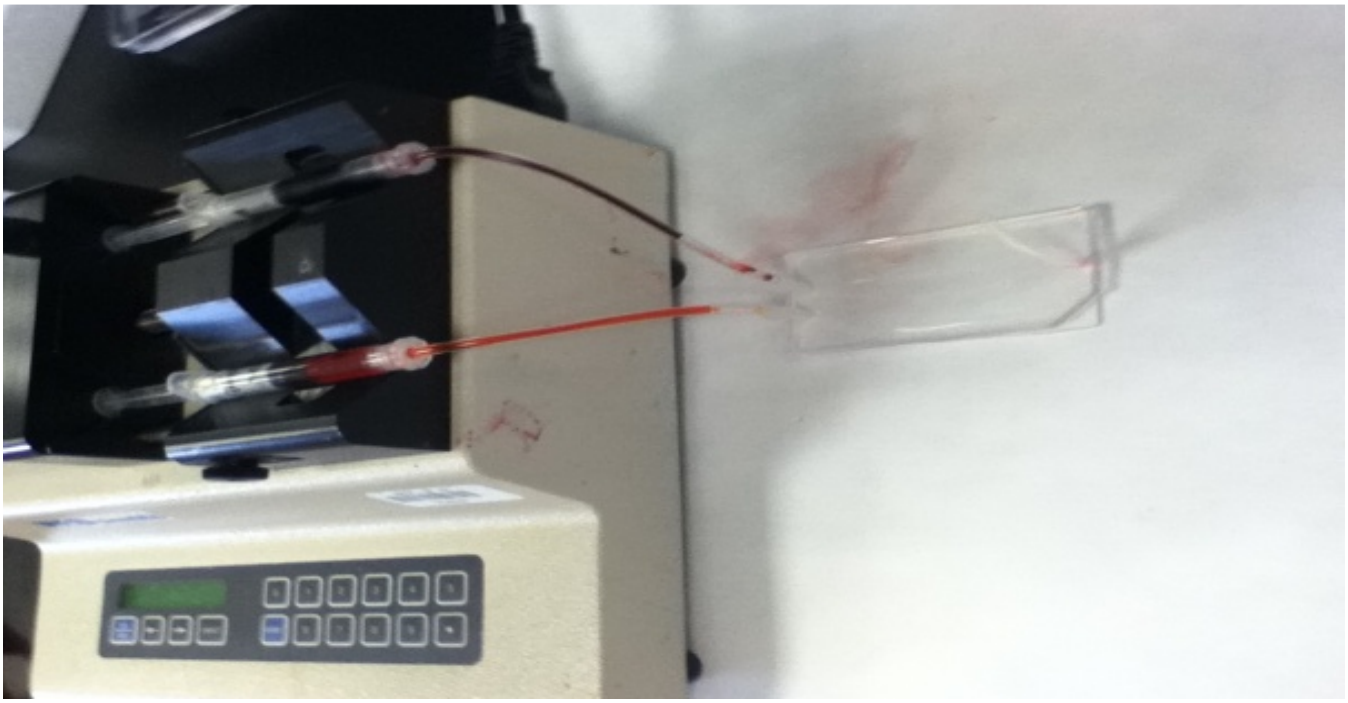

Figure 13: Dye Mixing Experimental Setup containing the red and yellow dye syringes fitted to the Flow Cell

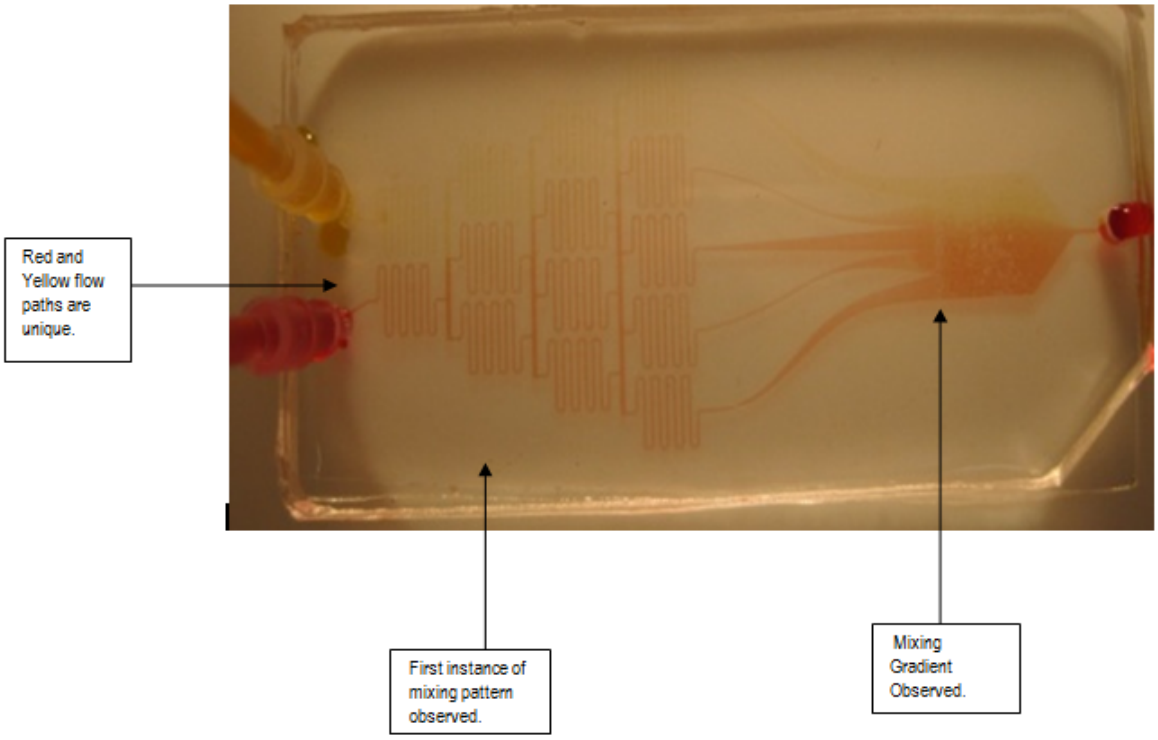

Figure 14: Observed Dye Mixing gradient inside the Porous Media Graduated Bands changing colors from Yellow→ Orange→ Red entering from the tortuous channels on the left.

The dye mixing experiments served as tracer test for further chemical gradient driven experiments. The diffusive channel length in the flow cell consists of 4 segments (Figure 11) before all the 5 inlets enter the porous media. In the first segment, the Red and Yellow colors enter independently. The end of first segment can be identified (Figure 13) as containing equal concentrations of red and yellow. When viewed under simple microscope, the channel consisted of 2 parallel streams of Yellow and Red flowing side by side. We observed the first instance of mixing starting to appear at the end of this second segment. In the following segments, Red was prominent in the lowermost channel entering the porous media and Yellow in the upper most. The center most inlet channel consisted Orange colored fluid entering the porous media. Inside the porous media, original streams were

preserved in the lowermost and uppermost extremes while a gradient in Orange was observed in the central band. There was no gradient observed lateral to the flow through the porous media in the flow cell which was evident from the preserved streams of Yellow and Red inside the porous media.

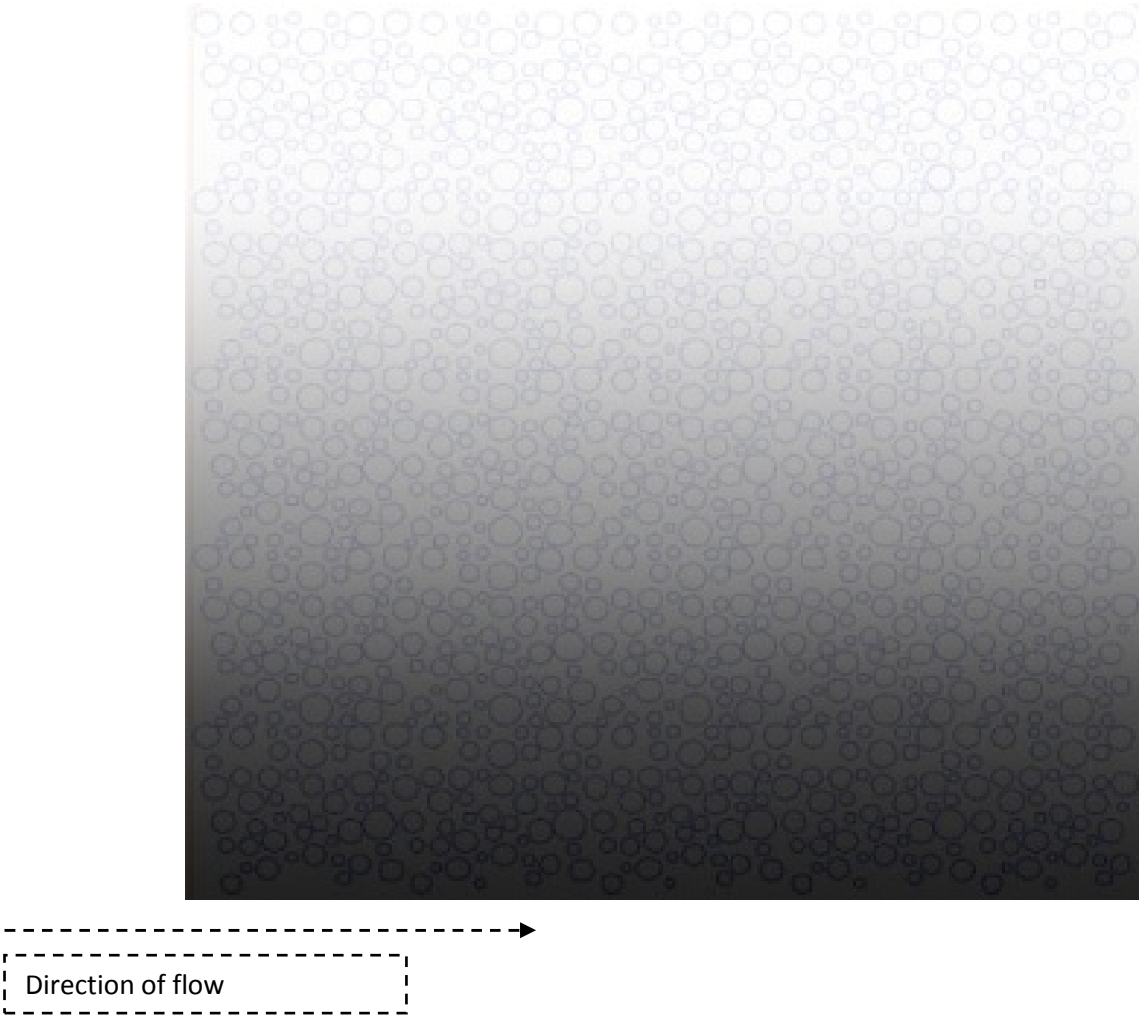

Figure 15: Simulation of dye mixing gradient by superimposing the gradient scheme on the AutoCAD drawing of the porous media in Adobe Photoshop CS5.1

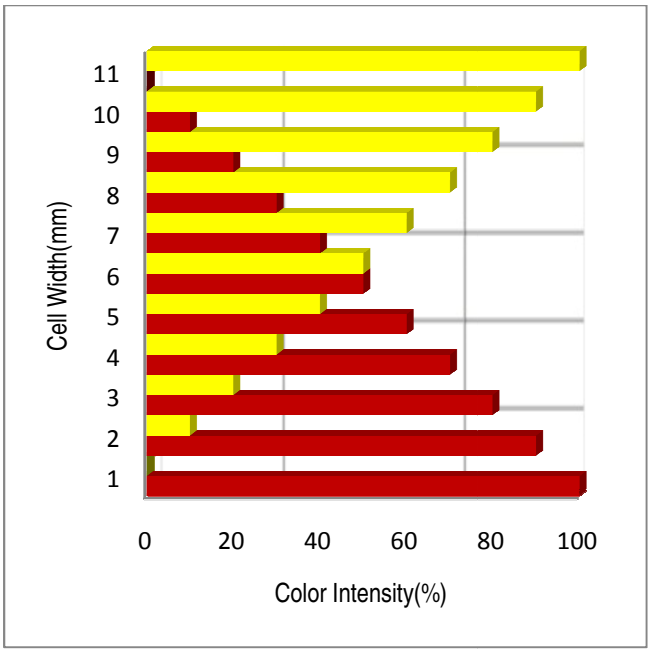

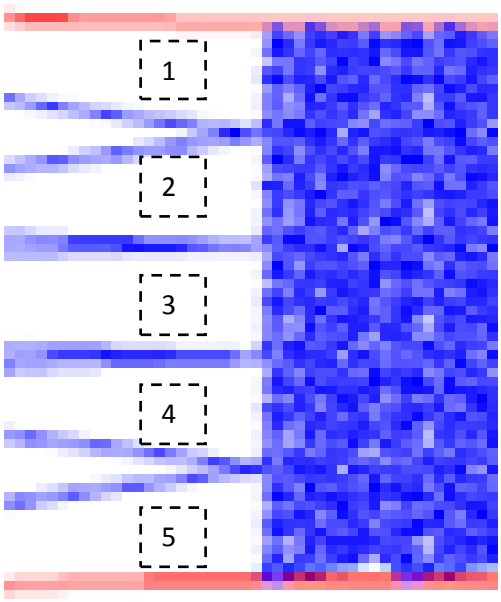

Figure 16: Observed Diffusion Gradient- estimated distribution of individual color intensities across the width of the porous media. Image on Right indicates the position of the 5 inlet channels entering the porous media. (Cropped and Magnified Image: Figure 11)

Direct quantification of color intensity analysis from the gradient observed under the microscope was not possible with image analysis due to two reasons. Firstly, poor resolution monochrome data available from the microscope camera images did not allow us to capture the exact gray scale variations along the gradient. Secondly, due to the relatively large dimensions of the porous media (10mm *10mm), a snapshot of the entire mixing gradient could not be obtained from the microscope camera. Instead, a digital camera image of the flow cell (Figure 13) combined with visual observations under the simple microscope were used to simulate a perfect mixing regime inside the porous media. The dye mixing observed inside the flow cell was quantified by dividing the width (perpendicular to flow) 10 mm into 5, 2mm wide rows which received input from 1 inlet channel each.(Ref: Figure 15-Right). Channel 1 was observed to contain Yellow stream only and Channel 5 contained Red stream only. The gradient in Orange developed in the channels 2, 3, and 4 with channel 3 showing maximum intensity of orange

color. This experiment allowed us to visually identify a single mixing band inside the porous media. Since the stream lines were preserved along the length of the porous media, we report that there was no lateral mixing in the porous media. A simulation of how the gradient might have looked if the entire porous media could be observed under the microscope was developed using Adobe Photoshop CS 5.1, Gradient tool (Figure 14)

The purpose of conducting the dye experiments was to identify the central mixing regime where there was a 50:50 mixing of the 2 influent solutions. The mixing and flow pattern observed inside the Flow Cell was in agreement with the theoretical calculations. Also, the travel time of the solutions through the diffusive mixing channel before it entered the porous media was under 10 minutes. An important parameter, the travel time through the mixing channel was required to be shorter in order to allow mixing induced chemical reactions to occur inside the porous media only and not within the mixing channels.

Diffusion Controlled Iron Oxidation Kinetics

Brief overview

The Flow Cell constructed with the mixing channel was used to understand and demonstrate diffusive mixing of solutions in microfluidic devices. Using dye mixing tracer tests, we were able to successfully set up a concentration gradient profile for the two influent solutions and observe the relative change in color intensity along the characteristic diffusive length inside the porous media. The dye test also allowed us to evaluate the time scales in which the chemical gradient was set up inside the region of interest (porous media).

Micromodels have been widely used to simulate the nutrient cycling dynamics in order to observe chemical reactions leading to particle interactions at a sub micron level. The Hyporheic zone has been our region of interest to study fresh water iron redox cycling that occurs at the interface due to dynamic mixing of the ground water and surface water bodies. The mixing of Fe (II) rich ground water with (O2) rich surface water is one such phenomenon that occurs at the interface zone. The location of iron oxide precipitation is regulated by the diffusion rates of Fe (II) (aq) and O2 (g) and thus elucidates the importance of interface properties and diffusive gradients on iron transformations in natural systems.

At near neutral pH, dissolved Fe (II) species in the oxic region of the sediment –water interface undergo rapid chemo-oxidation by dissolved O_2[42].

$$-\frac{d[Fe^{2+}]}{dt} = k[Fe^{2+}]\left[OH^{-}\right]\mathrm{P}_{O2} \qquad (7)$$

The rate constant k for Fe (II) oxidation is 1.5 (+- 0.5) * 10 13 l^3 mol^{-3} min^{-1} [43] A single Fe (II) may undergo transformations several times as it moves back and forth between aerobic and anaerobic regimes of the sediment water interface[44]. Fe (III) quickly hydrolyzes and precipitates as Fe (III) oxyhydroxides with the following general reaction thereby reducing the pH of the system:

$$Fe^{2+} + \left[\frac{1}{4}\right] O_2 + \left[\frac{5}{2}\right] H_2O \rightarrow Fe(OH)_3 + 2H^{+} \quad G\circ = -109 \text{ kJ mol}-1 \qquad (8)$$

The dye mixing experiments provided a qualitative measure of the two influent solutions which could be applied to anticipate the Fe-O_2 ratios that were incident at different locations inside the porous media. The Fe-O_2 ratios varied along the width of the cell (top to bottom) as (100-0, 90-10, 80-20 so on …0-100). With these relative ratios, the anticipated Fe-O_2 concentrations were calculated along the width of the cell.

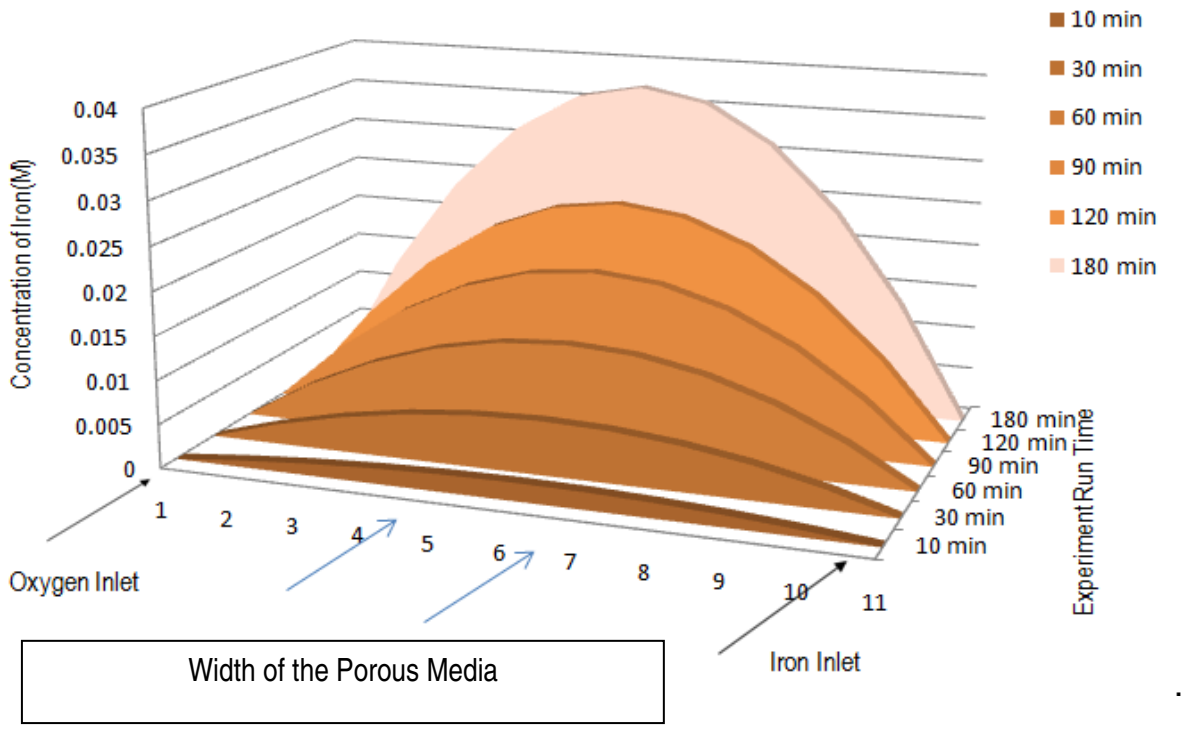

Figure 17: Expected distribution of freshly formed iron oxyhydroxides inside the porous media of the flow cell (Empirical- using [Fe (II)] = 0.002M and P_{O2}= 1.03atm, pH=7.5) [Fe (II): O2] mixing ratios obtained from the qualitative gradient observed in dye mixing experiment.

The anticipated distribution of freshly formed amorphous iron oxyhydroxides was calculated from iron oxidation kinetics (7) coupled with dye mixing observations. The pH was assumed to be 7.5 for calculation and the initial concentrations of Fe (II) and P_{O2} were 0.002M and 1.03 atm respectively (Table 5) to calculate the reaction rate. The expected distribution indicates maximum formation of iron oxyhydroxides in the center of the porous media

(Figure 16). With the travel time across the diffusive mixing channel being 10 minutes, it was safe to assume from reaction kinetics that there would be no oxidation of Fe (II) before the solutions entered the porous media.

We intend to simulate mixing induced iron oxidation inside the porous media of the Flow Cell and observe the distribution of the freshly formed amorphous iron oxyhydroxides based on the empirical calculations from reaction kinetics.

Methods

Cell Preparation

The iron oxidation experiments were performed in the same Flow Cell that was used for dye mixing experiments to preserve the exact location of the central mixing band identified with dyes. The Flow Cell was washed with blank solution of 5mM NaCl solution at the flow rate of 5μl/min for 60 min in order to remove air bubbles and dye particles.

Materials

A 0.002 M Iron (II) stock as prepared by dissolving ferrous ammonium sulfate hexahydrate (certified ACS crystalline: lot# 102325) in DI water (bubbled with N_2 gas; pH=8.5). Oxygenated water was prepared by bubbling DI water (bubbled with N_2 gas; pH=8.5) with pure O_2 gas (1atm) for 40 minutes.

Experimental Setup

The setup was similar to the dye mixing experiments with the syringes now replaced with the iron and oxygen stock solutions. The syringes were filled with respective stock solutions carefully, to avoid any air bubbles entering the flow paths. Syringe 1 containing Fe (II) was fitted on to the top inlet well of the device and Syringe 2 containing

oxygenated water was fitted on to the bottom inlet well of the device. The flow rate was set at 5µl/min and the experiment was run under the microscope for a period of 3 hrs 15 min.

Images were captured at regular intervals (0, 10,30,60,90,120,180 min) along the direction of the flow (Length: 0mm, 4mm, 9mm) of the central mixing band inside the porous media to observe the adsorption pattern of freshly formed amorphous oxyhydroxides to the PDMS "Beads" (Figure 17). The approximate coordinates for the images were obtained from the microscope controls. Although extreme care was taken to ensure that all images were captured at the same location, snap shots of the porous media could be captured at different times for image analysis. The main aim of presenting these images was to give the reader an idea of how the iron oxyhydroxides were formed and deposited at different distances from the inlets.

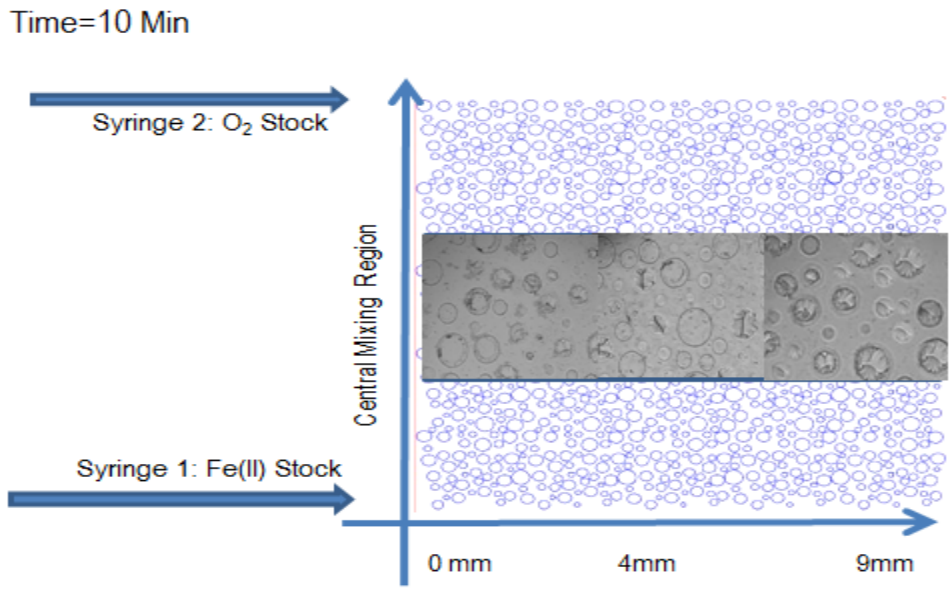

Figure 18: Experimental Setup indicating relative positions of the mixing regime inside the porous media and the location of iron and oxygen solutions inside the flow cell (Not to scale: depicts only porous media)

Results and Discussion

At 20 minutes of reaction progress, formation and subsequent deposition of iron oxyhydroxides was seen at the inlet of the porous media (Figure 19). The microscope controls were used to navigate and observe the formation of iron oxides inside the flow cell with the eye piece in order to observe the real process since the camera only produced monochrome images. The diffusive mixing channel was scanned under the eye piece to ensure clogging of channels due to iron solids. The microscope eye piece was scanned over the flow channels to ensure that there was no clogging inside the tortuous flow path. The absence of any oxides in the flow channels confirmed our calculations of reaction kinetics. The first instance of oxidation leading to the formation of orange colored amorphous iron solids was observed at (X =0 mm Y=5 mm) where X is the direction of flow and Y is the width of the cell (Figure 17). Collision with the PDMS "beads" led to deposition of the amorphous iron oxide particles around the surfaces. Negligible deposition was observed at the top and bottom regions of the porous media.

At the end of the experiment, a large amount of iron deposition was observed along the length of the central mixing band with maximum deposition near inlet and decreasing deposition along the length of the flow. We believe that the experimental run time was short to observe any repulsive interactions between the like charged iron oxyhydroxides and the deposition was predominated by the attractive forces between the negatively charged PDMS and positively charged iron oxyhydroxides. The relative distribution of freshly formed iron oxyhydroxides inside the central mixing regime over the entire experiment run time was calculated for the images collected at different time intervals. A distinct pattern was observed in along (X: 1, 4, 9 mm and Y: 5 mm) approximately, increase in particle deposition with increase in reaction time was analyzed only for this region. The number of beads covered with iron oxyhydroxides was calculated in Adobe Photoshop CS5.1 using the same approach followed for iron transport experiments (Section 4).

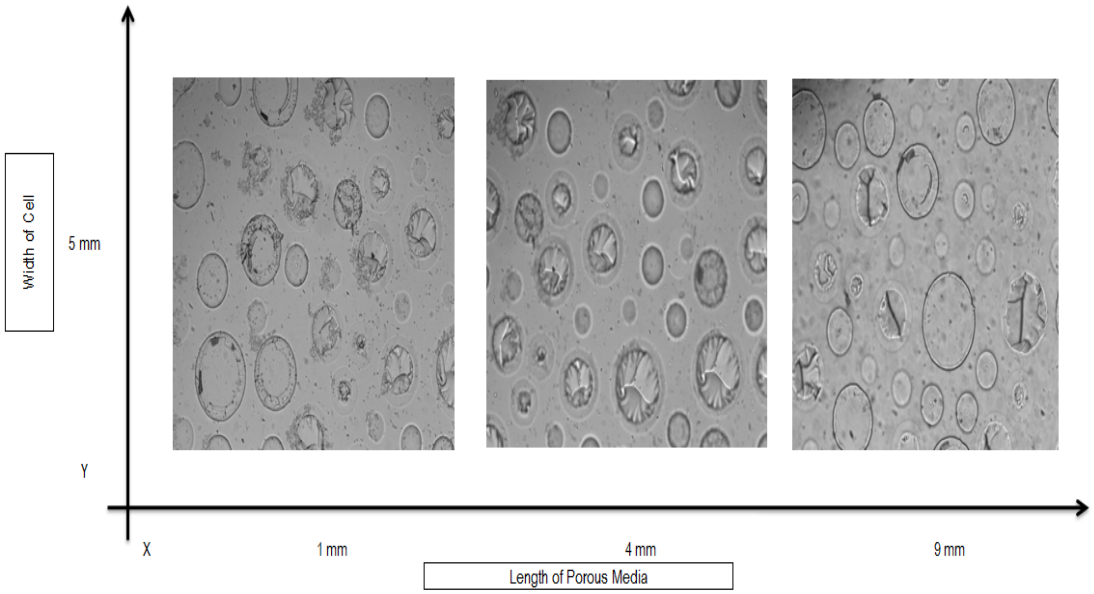

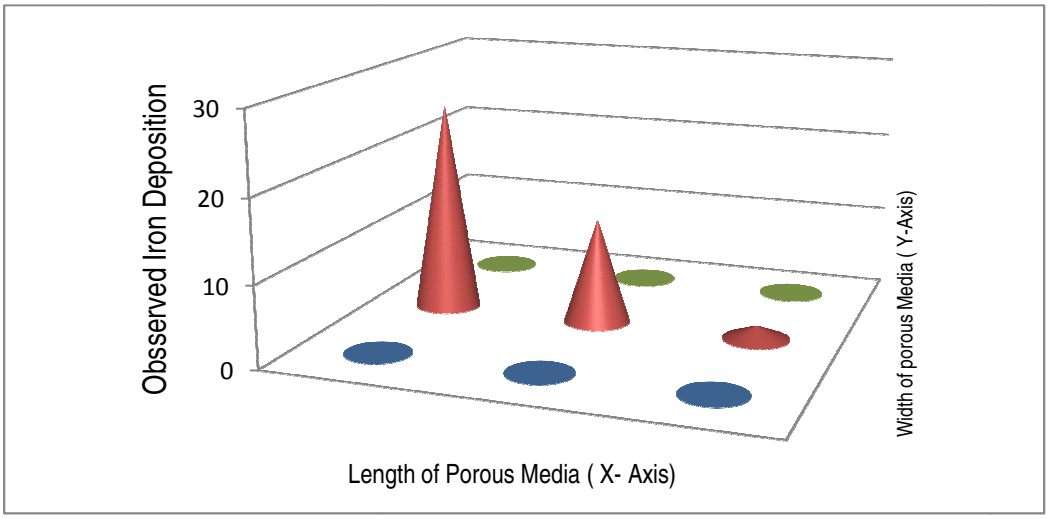

Figure 19: Observed Iron Oxide Depositions (using [Fe (II)] = 0.002M and P_{O2}= 1.03atm, Reaction time=20 minutes) [Approximate Coordinates of Images {X, Y} = {(X: 1 mm, 4 mm, 9 mm), Y: 5 mm}] (Approximate location of the orange band seen inside the porous media during dye experiments. The area plot indicates the relative deposition trend observed inside the cell where the floor indicates 2-D view of the porous media and colored cones indicate the qualitative concentrations calculated as % beads covered.

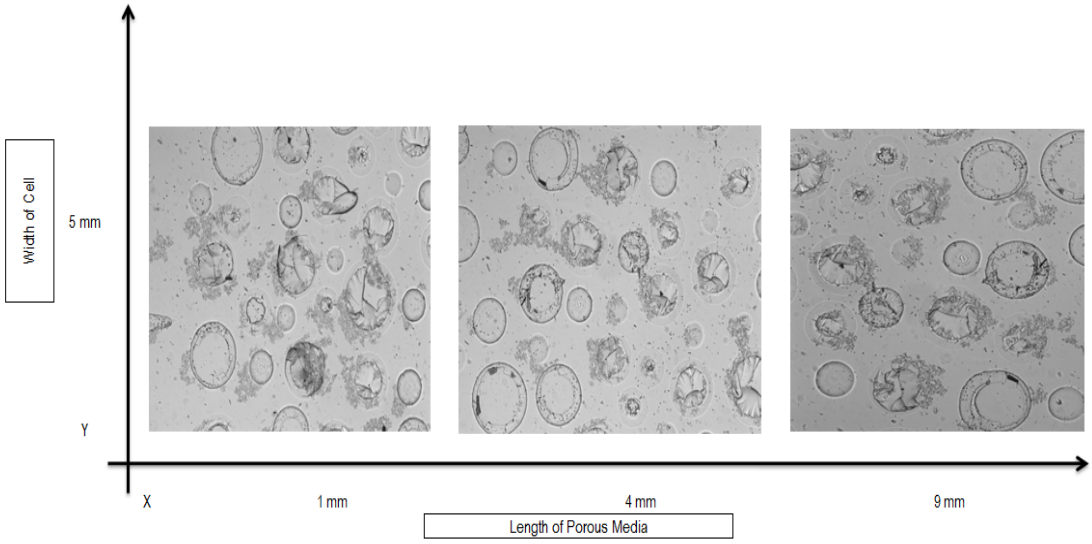

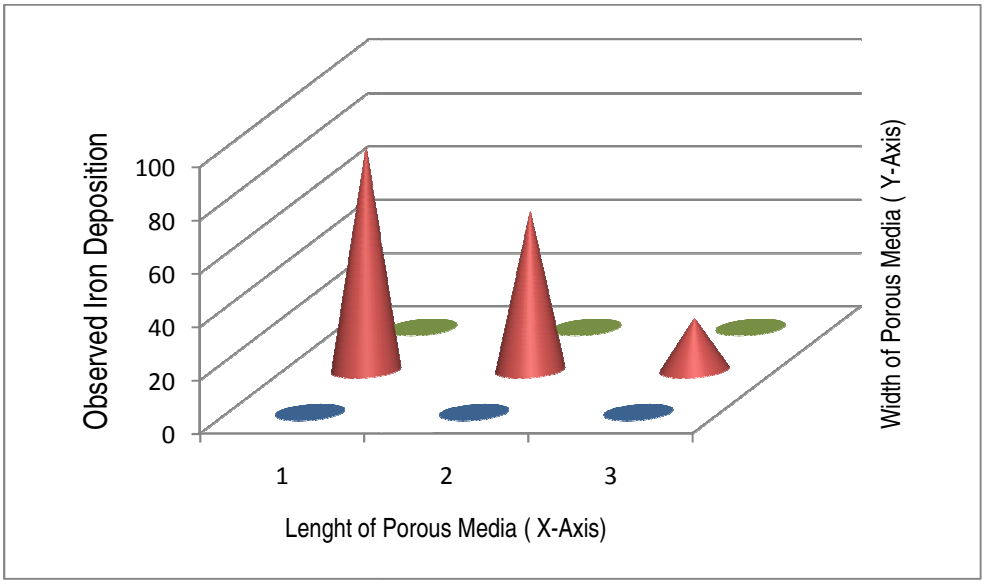

Figure 20: Observed Iron Oxide Depositions (using [Fe (II)] = 0.002M and P_{O2}= 1.03atm, Reaction time=180 minutes) [Approximate Coordinates of Images {X, Y} = {(X: 1 mm, 4 mm, 9 mm), Y: 5 mm}] (Approximate location of the orange band seen inside the porous media during dye experiments. The area plot indicates the relative deposition trend observed inside the cell where the floor indicates 2-D view of the porous media and colored cones indicate the qualitative concentrations calculated as % beads covered

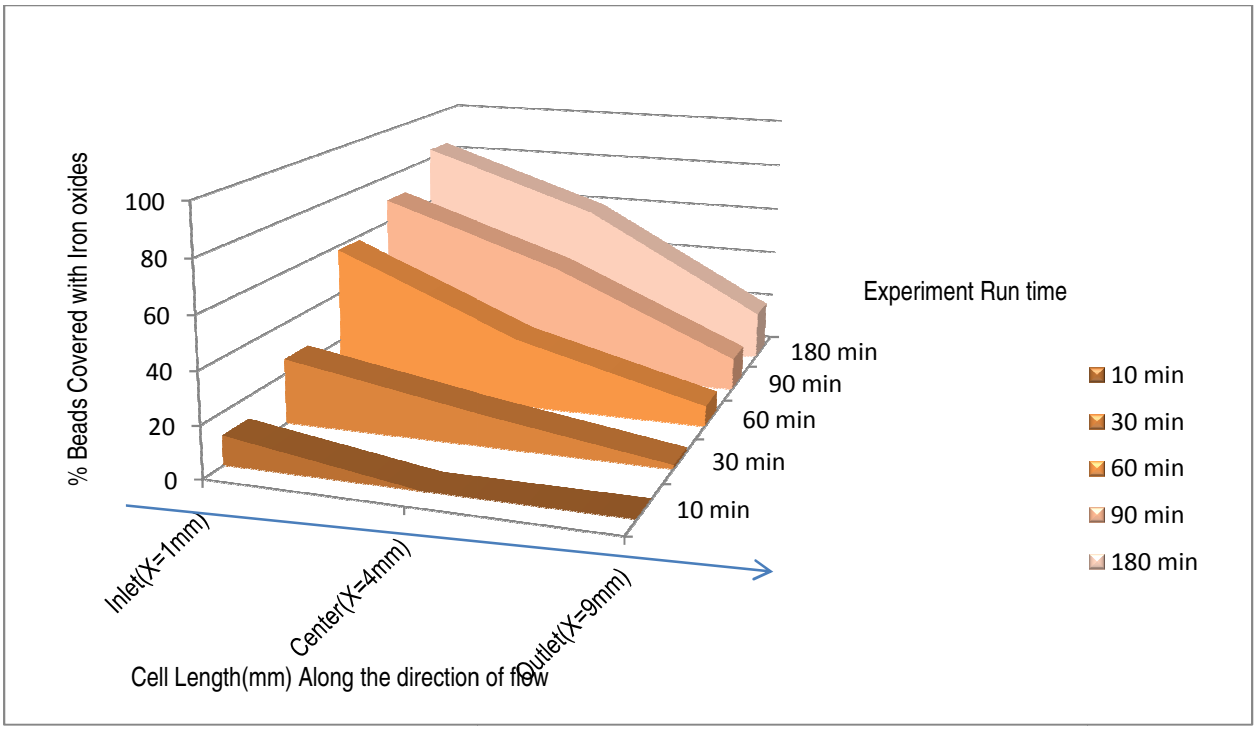

Figure 21: Observed deposition trend of freshly formed amorphous iron oxyhydroxides along the direction of flow (using [Fe (II)] = 0.002M and P_{O2}= 1.03atm) – calculated by counting ratio of iron coated beads to uncoated beads at different reaction times)

In our experiments, the formation of iron oxyhydroxides was observed within the first 20 minutes of experiment run time. The absence of any oxyhydroxides inside the diffusive mixing channels indicated negligible mixing of the two solutions before entering the porous media. Due to this, there was no clogging observed anywhere in the mixing channel. The presence of background electrolyte from the previous flushing of the flow cell only delayed the oxidation process inside the diffusive mixing length. In turn, the first instance of oxidation was observed right at the entrance of the porous media. Over the entire 180 minutes, maximum iron oxyhydroxides were found near the inlet with an increase seen in the direction of flow. This can be related from our past iron oxide transport experiments, where maximum deposition around the beads was seen close to the inlets. It should be noted that this method is only a qualitative presentation of the process and cannot be used to quantify the accurate

total iron deposited inside. Due to the relatively low volumes a spectrophotometric analysis of the effluent was not conducted.

Additional Observations

All solutions in the above experiments were prepared with DI water set to pH 8.5 in order to accommodate the reduction in pH due to formation of iron oxyhydroxides according to the following reaction:

$$Fe^{2+} + \left[\frac{1}{4}\right] O_2 + \left[\frac{5}{2}\right] H_2O \rightarrow Fe(OH)_3 + 2H^+ \qquad (7)$$

The final pH of the entering solutions inside the flow cell must have been near neutral since there was no oxidation observed inside the flow cell within the first 20 minutes. The travel time across the diffusive mixing channel was observed to be 10 minutes hence mixing inside the porous media started only at t=20 minutes. In another set of experiments, we observed that by lowering the starting pH from 8.5 to 6.9, there was no oxidation observed in the total reaction run time of 3 hours.

The reaction rate constant of iron oxidation is dependent on the pH of the system and is directly proportional to [**OH]** ²(7). On lowering the pH by 0.5 units, the half life value of the t1/2 of the oxidation reaction increased by a factor of 10. In our previous experiments, we observed iron oxidation to appear inside the porous media at t=20minutes which suggests that the pH of the system was around 7 since the t1/2 at that pH is around 23 minutes. In the second set of experiments, where the starting pH was 6.8, and there was further lowering of pH due to iron oxidation, the absence of any observed oxidation during the 3 hour reaction time suggested a reduction in kinetics of the reaction. This confirmatory test allowed us to understand the role of pH in reaction kinetics that continues to be valid even for microscale processes.

Conclusion

In this research we have demonstrated the applicability of Polydimethylsiloxane (PDMS) as a surrogate for glass or quartz to understanding the transport of iron oxide colloid particles in porous media. Our results indicate that PDMS can demonstrate surface properties that would enable us to model porous media. The zeta potential values of PDMS plasma cleaned for 25 seconds is well within the range of reported values for other forms of silica. Using AutoCAD, Ecochip –microfluidic cell containing pores and constrictions of porosity 49.43% allowed us to observe iron oxide transport in an artificial porous media. This arrangement allowed us to understand iron solid-silica interactions at micron scale resolution. The particle deposition rate and single collector efficiency were calculated from the influent and effluent sample concentrations. The last series of experiments were conducted using the Flow cell designed with AutoCAD at UCONN. The porosity of this cell was also 49.43% but in order to accommodate the diffusive mixing inlet channels and observe a good chemical gradient, the size was enlarged. A diffusive mixing induced chemical gradient was successfully set up inside the porous media which allowed simultaneous iron oxidation –deposition reactions to take place inside the cell. The surface characterization and iron transport experiments served as preliminary understanding of surface properties and particle interactions that govern transport of iron oxides in an engineered media. This understanding was later extended to include diffusive mixing induced iron oxidation and adsorption kinetics. We were able to simulate the effect of mixing oxygen rich water bodies with anoxic mineral (iron) rich ground water bodies that in turn represent an important aspect of biogeochemical iron cycling in the fresh water aquifers.

Future Work

In our experimental work, we were able to successfully demonstrate diffusive mixing induced iron oxidation and adsorption kinetics in an artificial porous media. The challenges involved in setting up the system allowed us to identify possible areas for extensive improvement. In our Flow Cell design, the height of the channels was chosen to be 17 microns, which was very low compared to the height of channels in the Ecochip (30 microns). We believe that such low channel heights when subjected to a constant flow rate at which our experiments were run could have been damaged or broken. This was observed in the low resolution images captured by the microscope. An improvement here could be to increase the channel height to the original Ecochip height. Another reason for observed shearing off of the channels could be due to the irregularities in the original master of the device. Due to time constraints, replicate masters could not be produced to verify the robustness of the channels. Using the same flow cell for setting up chemical gradient followed by iron oxidation kinetics ensured that the gradient set up with dye mixing could be applied to the iron oxidation experiments also. This approach although valid only doubled the total exposure time of the device to a constant flow rate i.e. the device was under a constant flow through system for 7 hours which included 3 hours of dye mixing, 1 hour of background flushing and 3 hours of iron oxidation kinetics. We believe that this might have introduced mechanical jerks due to constant plugging of the tube fittings. An ideal method here would be to use separate devices for both experiments which is possible if the mixing gradient can be set up exactly identical for all devices.

The microscope used for our image acquisition was equipped with a monochrome camera only. Image analysis for quantifying iron oxides was challenging due to low resolution data of the amorphous oxides. An improvement here would be either to obtain color images or to develop a contrast technique to capture iron oxides only.

Finally, iron oxidation kinetics could be experimentally studied for only 1 concentration scenario of iron-oxygen mixing. An extension would be study the effect of varying oxygen concentration on the reaction kinetics. This in turn would complete our representation of the iron oxidation at the interface zone where a steep oxygen gradient modulates iron oxidation mechanism. This experiment can be used to understand the effect of biological activity that mediates fresh water iron cycling.

References

1. Triska, F. J.; Duff, J. H.; Avanzino, R. J., The role of water exchange between a stream channel and its hyporheic zone in nitrogen cycling at the terrestrial-aquatic interface. *Hydrobiologia* **1993,** *251*, (1), 167-184.

2. Krause, S.; Hannah, D. M.; Fleckenstein, J. H., Hyporheic hydrology: interactions at the groundwater-surface water interface. *Hydrological Processes* **2009,** *23*, (15), 2103-2107.

3. Saenger, N.; Kitanidis, P. K.; Street, R. L., A numerical study of surface-subsurface exchange processes at a riffle-pool pair in the Lahn River, Germany. *Water Resour. Res.* **2005,** *41*, (12), W12424.

4. Boulton, A. J.; Findlay, S.; Marmonier, P.; Stanley, E. H.; Valett, H. M., The Functional Significance of the Hyporheic Zone in Streams and Rivers. *Annual Review of Ecology and Systematics* **1998,** *29*, 59-81.

5. Hucks Sawyer, A.; Bayani Cardenas, M.; Bomar, A.; Mackey, M., Impact of dam operations on hyporheic exchange in the riparian zone of a regulated river. *Hydrological Processes* **2009,** *23*, (15), 2129-2137.

6. Lewandowski, J.; Putschew, A.; Schwesig, D.; Neumann, C.; Radke, M., Fate of organic micropollutants in the hyporheic zone of a eutrophic lowland stream: Results of a preliminary field study. *Science of The Total Environment 409*, (10), 1824-1835.

7. Boano, F.; Packman, A. I.; Cortis, A.; Revelli, R.; Ridolfi, L., A continuous time random walk approach to the stream transport of solutes. *Water Resour. Res.* **2007,** *43*, (10), W10425.

8. Christensen, T. H.; Kjeldsen, P.; Bjerg, P. L.; Jensen, D. L.; Christensen, J. B.; Baun, A.; Albrechtsen, H.-J.; Heron, G., Biogeochemistry of landfill leachate plumes. *Applied Geochemistry* **2001,** *16*, (7-8), 659-718.

9. Borch, T.; Masue, Y.; Kukkadapu, R. K.; Fendorf, S., *Environ. Sci. Technol.* **2007,** *41*, (null), 166.

10. Emerson, D.; Revsbech, N. P., Investigation of an Iron-Oxidizing Microbial Mat Community Located near Aarhus, Denmark: Field Studies. *Appl. Environ. Microbiol.* **1994,** *60*, (11), 4022-4031.

11. Neubauer, S. C.; Emerson, D.; Megonigal, J. P.; Violante, A.; Huang, P. M.; Gadd, G. M., *Biophysico-Chemical Processes of Heavy Metals and Metalloids in Soil Environments*. 2008; p 339.

12. Druschel, G. K.; Emerson, D.; Sutka, R.; Suchecki, P.; Luther Iii, G. W., Low-oxygen and chemical kinetic constraints on the geochemical niche of neutrophilic iron(II) oxidizing microorganisms. *Geochimica et Cosmochimica Acta* **2008,** *72*, (14), 3358-3370.

13. Straub, K. L.; Rainey, F. A.; Widdel, F., *Int J Syst Bacteriol* **1999,** *49*, 729.

14. Bruun, A.-M.; Finster, K.; Gunnlaugsson, H. P.; NâŠ˜rnberg, P.; Friedrich, M. W., A Comprehensive Investigation on Iron Cycling in a Freshwater Seep Including Microscopy, Cultivation and Molecular Community Analysis. *Geomicrobiology Journal 27*, (1), 15-34.

15. McCarthy, J. F.; Zachara, J. M., *Environ. Sci. Technol.* **1989,** *23*, (null), 496.

16. Kanti Sen, T.; Khilar, K. C., Review on subsurface colloids and colloid-associated contaminant transport in saturated porous media. *Advances in Colloid and Interface Science* **2006,** *119*, (2-3), 71-96.

17. Gan, P.; Yu, R.; Smets, B. F.; MacKay, A. A., Sampling methods to determine the spatial gradients and flux of Arsenic at a groundwater seepage zone. *Environmental Toxicology and Chemistry* **2006,** *25*, (6), 1487-1495.

18. Ryan, J. N.; Elimelech, M., *Colloid Surf. A* **1996,** *107*, (null), 1.

19. Zhang, C.; Dehoff, K.; Hess, N.; Oostrom, M.; Wietsma, T. W.; Valocchi, A. J.; Fouke, B. W.; Werth, C. J., Pore-Scale Study of Transverse Mixing Induced CaCO3 Precipitation and Permeability Reduction in a Model Subsurface Sedimentary System. *Environmental Science & Technology 44*, (20), 7833-7838.

20. Sirivithayapakorn, S.; Keller, A., Transport of colloids in saturated porous media: A pore-scale observation of the size exclusion effect and colloid acceleration. *Water Resour. Res.* **2003,** *39*, (4), 1109.

21. McDowell-Boyer, L. M.; Hunt, J. R.; Sitar, N., Particle transport through porous media. *Water Resour. Res.* **1986,** *22*, (13), 1901-1921.

22. Grolimund, D.; Elimelech, M.; Borkovec, M.; Barmettler, K.; Kretzschmar, R.; Sticher, H., *Environ. Sci. Technol.* **1998,** *32*, (null), 3562.

23. Duffy, D. C.; McDonald, J. C.; Schueller, O. J. A.; Whitesides, G. M., Rapid Prototyping of Microfluidic Systems in Poly(dimethylsiloxane). *Analytical Chemistry* **1998,** *70*, (23), 4974-4984.

24. Stumm, W., *Chemistry of the Solid-Water Interface*. 1992; p null.

25. Delgado, A. V.; González-Caballero, F.; Hunter, R. J.; Koopal, L. K.; Lyklema, J., Measurement and interpretation of electrokinetic phenomena. *Journal of Colloid and Interface Science* **2007,** *309*, (2), 194-224.

26. Eggleston, C.; Jordan, G., A new approach to pH of point of zero charge measurement: crystal-face specificity by scanning force microscopy (SFM). *Geochimica et Cosmochimica Acta* **1998,** *62*, (11), 1919-1923.

27. Sharma, M. M.; Yen, T. F., Interfacial electrochemistry of oxide surfaces in oil-bearing sands and sandstones. *Journal of Colloid and Interface Science* **1984,** *98*, (1), 39-54.

28. Kosmulski, M., A literature survey of the differences between the reported isoelectric points and their discussion. *Colloids and Surfaces A: Physicochemical and Engineering Aspects* **2003,** *222*, (1-3), 113-118.

29. Hollahan, J. R.; Carlson, G. L., Hydroxylation of polymethylsiloxane surfaces by oxidizing plasmas. *Journal of Applied Polymer Science* **1970,** *14*, (10), 2499-2508.

30. Hillborg, H.; Gedde, U. W., Hydrophobicity recovery of Polydimethylsiloxane after exposure to corona discharges. *Polymer* **1998,** *39*, (10), 1991-1998.

31. Owen, M. J.; Smith, P. J., Plasma treatment of Polydimethylsiloxane. *Journal of Adhesion Science and Technology* **1994,** *8*, (10), 1063-1075.

32. KIRB (Iron Reducing Bacteria)y, B. J.; Hasselbrink, E. F., Zeta potential of microfluidic substrates: 1. Theory, experimental techniques, and effects on separations. *ELECTROPHORESIS* **2004,** *25*, (2), 187-202.

33. Stephan, E. A.; Chase, G. G., A preliminary examination of zeta potential and deep bed filtration activity. *Separation and Purification Technology* **2001,** *21*, (3), 219-226.

34. Gu, Y.; Li, D., The [zeta]-Potential of Glass Surface in Contact with Aqueous Solutions. *Journal of Colloid and Interface Science* **2000,** *226*, (2), 328-339.

35. Kuhnen, F.; Barmettler, K.; Bhattacharjee, S.; Elimelech, M.; Kretzschmar, R., Transport of Iron Oxide Colloids in Packed Quartz Sand Media: Monolayer and Multilayer Deposition. *Journal of Colloid and Interface Science* **2000,** *231*, (1), 32-41.

36. Elimelech, M.; O'Melia, C. R., *Langmuir* **1990,** *6*, (null), 1153.

37. Yao, K.-M.; Habibian, M. T.; O'Melia, C. R., Water and waste water filtration. Concepts and applications. *Environmental Science & Technology* **1971,** *5*, (11), 1105-1112.

38. Tufenkji, N.; Elimelech, M., Deviation from the Classical Colloid Filtration Theory in the Presence of Repulsive DLVO Interactions. *Langmuir* **2004,** *20*, (25), 10818-10828.

39. Yao, K. M.; Habibian, M. T.; O'Melia, C. R., *Environ. Sci. Technol.* **1971,** *5*, (null), 1105.

40. Cornell, R. M.; Schwertmann, U., *The iron oxidesâ€"Structure, Properties, Reactions, Occurrence and Uses*. 1996.

41. Stookey, L. L., Ferrozine---a new spectrophotometric reagent for iron. *Analytical Chemistry* **1970,** *42*, (7), 779-781.

42. Davison, W.; Seed, G., The kinetics of the oxidation of ferrous iron in synthetic and natural waters. *Geochimica et Cosmochimica Acta* **1983,** *47*, (1), 67-79.

43. Hug, S. J.; Leupin, O., *Environ. Sci. Technol.* **2003,** *37*, (null), 2734.

44. Van Cappellen, P.; Wang, Y., Cycling of iron and manganese in surface sediments; a general theory for the coupled transport and reaction of carbon, oxygen, nitrogen, sulfur, iron, and manganese. *Am J Sci* **1996,** *296*, (3), 197-243.

Appendix 1

Ecochip Construction

Silicon Master Fabrication:

The AutoCAD drawing (Ref: Figure 7) was transferred to the surface of silicon wafer using the soft photolithographic process consisting of the following steps: (**SU-8 2000 Permanent Epoxy Negative Photoresist PROCESSING GUIDELINES FOR:SU-8 2025, SU-8 2035, SU-8 2050 and SU-8 2075**)

a) Substrate preparation – to obtain reliability of the final device, the substrate was etched using H2SO4 or H2O2 followed by DI water rinse.
b) Application of thin uniform layer of Photoresist (SU8) - by high speed centrifugal whirling of silicon wafers called Spin Coating
c) Soft baking- to make the Photoresist coating photosensitive
d) Hard baking- to harden the Photoresist and improve adhesion to wafer surface

PDMS Preparation:

PDMS and Curing agent from Sylgard (R) 184 Silicone Elastomer Kit (which includes Base and Curing Agent) from Dow Corning Corporation, Midland, MI were prepared mixing in a 10:1 base to curing agent ratio to prepare the PDMS. This mixture was thoroughly mixed for approximately 3 minutes and placed inside the degasser in vacuum for approximately 15 minutes to remove air bubbles.

Ecochip Device Casting:

The final device was cast under bio safety hood by pouring the degassed PDMS mixture over the silicon master and degassed again for 15-20 minutes to remove any air bubbles over the device. After pouring, the device was cured at 60^0C for minimum of 2 hours. Once the device was ready, it was carefully cut out of the master and stored in a clean petridish. The inlet and outlet holes were punched into the device using biopsy punches prior to plasma bonding. The device was cleaned with isopropyl alcohol and dried with N_2 gas and plasma bonded to a methanol cleaned glass slide. The device was then filled with DI water to retain the hydrophilic property achieved through Oxygen plasma exposure for 25 seconds. The final porosity of the Ecochip was calculated to be 49.43% which was within the typical natural media regime.

Flow Cells were constructed using the above mentioned fabrication and casting protocol. The AutoCAD drawing was changed to include the diffusive mixing channel and larger dimension porous media as per experiment requirements.

Appendix 2

Tables

Table 1: Effect of Oxygen Plasma Exposure Time on Zeta Potential

Zeta Potential(mV) vs. pH

pH	***Planar Sample - Not Cleaned***	***Planar Sample (Plasma Cleaned 25Sec)***	***Planar Sample (Plasma Cleaned 30Sec)***	***Planar Sample (Plasma Cleaned 60Sec)***
4.5	-8.5	-19.5	-23.5	-28.5
5	-9.35	-21.5	-24	-30.2
5.5	-10.2	-23.4	-26.5	-34.5
6	-10.75	-25.25	-27.8	-38.4
6.5	-11.8	-26.4	-29.25	-42.75
7	-12.14	-27.6	-30.27	-46.52
7.5	-12.8	-28.7	-30.52	-47.25
8	-13.2	-30.2	-31.57	-50.45

Table 2: Effect of Sample Geometry on Zeta Potential

Zeta Potential (mV) vs. pH

pH	***Planar Sample (Plasma Cleaned 25Sec)***	***Packed 2mm cubes Sample(Plasma Cleaned 25Sec)***
4.5	-19.5	-23.5
5	-21.5	-24
5.5	-23.4	-26.5
6	-25.25	-27.8
6.5	-26.4	-29.25
7	-27.6	-30.27
7.5	-28.7	-30.52
8	-30.2	-31.57

Table 3: Comparison of Zeta Potential of Different Forms of Silica

pH	***Concrete Sand from Desiato's Sand and Gravel, Storrs CT***	***Ottawa Sand***	***Glass Beads 2mm***	***Planar Sample (Plasma Cleaned 25Sec)***
4.5	-10.75	-13.25	-18.5	-19.5
5	-11.5	-14.8	-20.5	-21.5
5.5	-14	-16.35	-21.44	-23.4
6	-17.25	-18.5	-23.25	-25.25
6.5	-20.2	-21.75	-24.8	-26.4
7	-21.5	-22.44	-25.75	-27.6
7.5	-23	-24.2	-27.45	-28.7
8	-24.3	-26.63	-28.5	-30.2

Table 4: Observed Iron Oxide Depositions on PDMS Beads

Total Number of Beads 62

Time	Number of Beads with Iron Deposition	Iron Accumulation over "Beads"
0	0	0
30	21	0.338709677
60	35	0.564516129
90	45	0.725806452
120	62	1
180	62	1

Table 5: Estimation of Iron Oxidation Rate Constant based on pH

Iron(II) M	DO mg/L	DO M	Partial Pressure of DO atm	pH	pH	pOH=14-pH	Oxidation rate constant(where k= k = 1.5 (+/-0.5) X10^13 L^3 mol^-3 min^-1)
$[Fe^{2+}]$	$[O_2]$	$[O_2]$	$p_{O2}=[O_2]/K_H$		$[H^+]$	$[OH^-]$	-d[Fe(II)]/dt = k * [Fe(II)]* P-O2* [OH-]^2
0.002	41.6	0.0013	1.032627	5.5	3.16228E-06	3.16228E-09	3.09788E-07
0.002	41.6	0.0013	1.032627	6.5	3.16228E-07	3.16228E-08	3.09788E-05
0.002	41.6	**0.0013**	**1.032627**	7.5	**5.62341E-08**	**1.77828E-07**	**0.000979636**
0.002	41.6	0.0013	1.032627	8.5	3.16228E-09	3.16228E-06	0.309788012

Table 6: Estimated Iron Oxide Concentrations along the width of the flow cell (calculated from reaction kinetics relation)

Length (mm)	Time					
	10 min	30 min	60 min	90 min	120 min	180 min
0.1	4.12086E-07	1.24E-06	2.47E-06	3.71E-06	4.94503E-06	7.42E-06
1	0.000741462	0.002224	0.004449	0.006673	0.008897541	0.013346
2	0.001318493	0.003955	0.007911	0.011866	0.015821917	0.023733
3	0.001730682	0.005192	0.010384	0.015576	0.020768183	0.031152
4	0.001978028	0.005934	0.011868	0.017802	0.023736337	0.035605
5	0.002060532	0.006182	0.012363	0.018545	0.024726382	0.03709
6	0.001978193	0.005935	0.011869	0.017804	0.023738316	0.035607
7	0.001731012	0.005193	0.010386	0.015579	0.020772139	0.031158
8	0.001318988	0.003957	0.007914	0.011871	0.015827851	0.023742
9	0.000742121	0.002226	0.004453	0.006679	0.008905454	0.013358
10	4.12086E-07	1.24E-06	2.47E-06	3.71E-06	4.94503E-06	7.42E-06

Table 7: Observed Iron Deposition inside Flow Cell –Calculated by Counting Number of beads with iron coating with respect to the total number of beads along the direction of flow (Inlet-→ Outlet)

% Bead Deposition over reaction time- calculated using Photoshop Image Analysis

		Inlet(X=1mm)	Center(X=4mm)	Outlet(X=9mm)
Time(min)	10 min	11.29032258	0	0
	30 min	25.80645161	12.90322581	1.612903226
	60 min	58.06451613	27.41935484	8.064516129
	90 min	69.35483871	45.16129032	12.90322581
	180 min	83.87096774	59.67741935	19.35483871

Appendix 3 (SurPASS Analyzer instrument manual for sample preparation)

Setup for Planar samples in a Clamping Cell Arrangement –Sample preparation

Set up for Cylindrical Cell Arrangement –Sample preparation

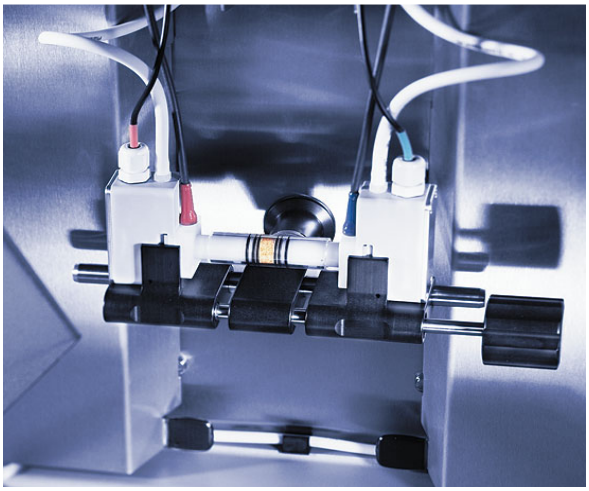

Experimental Set up inside the analyzer